Stem Cell Reports
Article

OPEN ACCESS

Exosome-Mediated Benefits of Cell Therapy in Mouse and Human Models of Duchenne Muscular Dystrophy

Mark A. Aminzadeh,[1] Russell G. Rogers,[1] Mario Fournier,[1] Rachel E. Tobin,[1] Xuan Guan,[2] Martin K. Childers,[2] Allen M. Andres,[1] David J. Taylor,[1] Ahmed Ibrahim,[1] Xiangming Ding,[3] Angelo Torrente,[1] Joshua M. Goldhaber,[1] Michael Lewis,[1] Roberta A. Gottlieb,[1] Ronald A. Victor,[1] and Eduardo Marbán[1,*]

[1]Smidt Heart Institute, Cedars-Sinai Medical Center, 8700 Beverly Boulevard, Suite AHSP 3100, Los Angeles, CA 90048, USA
[2]Institute for Stem Cell and Regenerative Medicine, University of Washington, Seattle, WA 98109, USA
[3]UCLA Technology Center for Genomics & Bioinformatics, Los Angeles, CA 90095, USA
*Correspondence: eduardo.marban@cshs.org
https://doi.org/10.1016/j.stemcr.2018.01.023

SUMMARY

Genetic deficiency of dystrophin leads to disability and premature death in Duchenne muscular dystrophy (DMD), affecting the heart as well as skeletal muscle. Here, we report that clinical-stage cardiac progenitor cells, known as cardiosphere-derived cells (CDCs), improve cardiac and skeletal myopathy in the *mdx* mouse model of DMD. Injection of CDCs into the hearts of *mdx* mice augments cardiac function, ambulatory capacity, and survival. Exosomes secreted by human CDCs reproduce the benefits of CDCs in *mdx* mice and in human induced pluripotent stem cell-derived Duchenne cardiomyocytes. Surprisingly, CDCs and their exosomes also transiently restored partial expression of full-length dystrophin in *mdx* mice. The findings further motivate the testing of CDCs in Duchenne patients, while identifying exosomes as next-generation therapeutic candidates.

INTRODUCTION

Absence of dystrophin in Duchenne muscular dystrophy (DMD) leads to membrane fragility and secondary damage to muscle (both skeletal and cardiac) (Shirokova and Niggli, 2013). Early disability is due predominantly to the skeletal myopathy, but heart failure is the most common cause of death (Verhaert et al., 2011). Cardiosphere-derived cells (CDCs) may represent a viable therapeutic option. CDCs are progenitor cells intrinsic to the heart; in clinical trials after myocardial infarction, CDCs promote cardiomyogenesis and reverse established scar (Makkar et al., 2012; Malliaras et al., 2014). Multiple lines of evidence now indicate that most of the beneficial effects of CDCs are indirect. In the extreme, allogeneic CDCs are cleared completely within several weeks, but their functional and structural benefits persist for at least 6 months (Malliaras et al., 2012). CDCs secrete diffusible factors that promote angiogenesis, recruit endogenous progenitor cells, and coax surviving heart cells to proliferate (Chimenti et al., 2010; Li et al., 2010); transplanted CDCs suppress maladaptive remodeling (Lee et al., 2011), apoptosis (Cheng et al., 2012; Li et al., 2010), fibrosis (Tseliou et al., 2013), and inflammation after myocardial infarction (Tseliou et al., 2013) and in non-ischemic cardiomyopathy (Aminzadeh et al., 2015b). These diverse mechanisms appear to be mediated via the secretion of exosomes laden with noncoding RNA, including microRNAs (miRNAs) (Ibrahim et al., 2014), consistent with the notion that exosomes contain a plethora of bioactive molecules that target multiple signaling pathways synergistically (Vyas and Dhawan, 2016). In a murine model of myocardial infarction, CDC-secreted exosomes (CDC exosomes) mimic the functional and structural benefits of CDCs, while blockade of exosome biosynthesis renders CDCs ineffective (Ibrahim et al., 2014). Given the clinical data with CDCs, and the complementarity between their therapeutic actions and the pathophysiological processes underlying Duchenne cardiomyopathy (oxidative stress [Menazza et al., 2010; Williams and Allen, 2007], inflammation [Wehling-Henricks et al., 2010], fibrosis [Tandon et al., 2015], and mitochondrial dysfunction [Burelle et al., 2010]), we reasoned that CDCs and their exosomes might be useful in treating Duchenne cardiomyopathy. Our early work reported in abstract form (Aminzadeh et al., 2014, 2015a) revealed striking phenotypic correction by CDCs in *mdx* dystrophic mice, motivating the HOPE-Duchenne clinical trial (Ascheim and Jefferies, 2016) of CDCs in DMD patients. Initially, we had not aspired to restore skeletal muscle function, but merely to offset the pathophysiological consequences of dystrophin deletion in the heart. We now report that CDCs and their secreted exosomes potently improve not only cardiac but also skeletal muscle structure and function, contributing to major systemic benefits after injection of CDCs into the heart. An unanticipated, minor restoration of dystrophin expression was also observed, but this cannot explain all of the observed benefits.

RESULTS

CDC Transplantation in *mdx* Hearts

Intramyocardial injection of first and second (lower) doses of CDCs into the hearts of *mdx* mice improved left

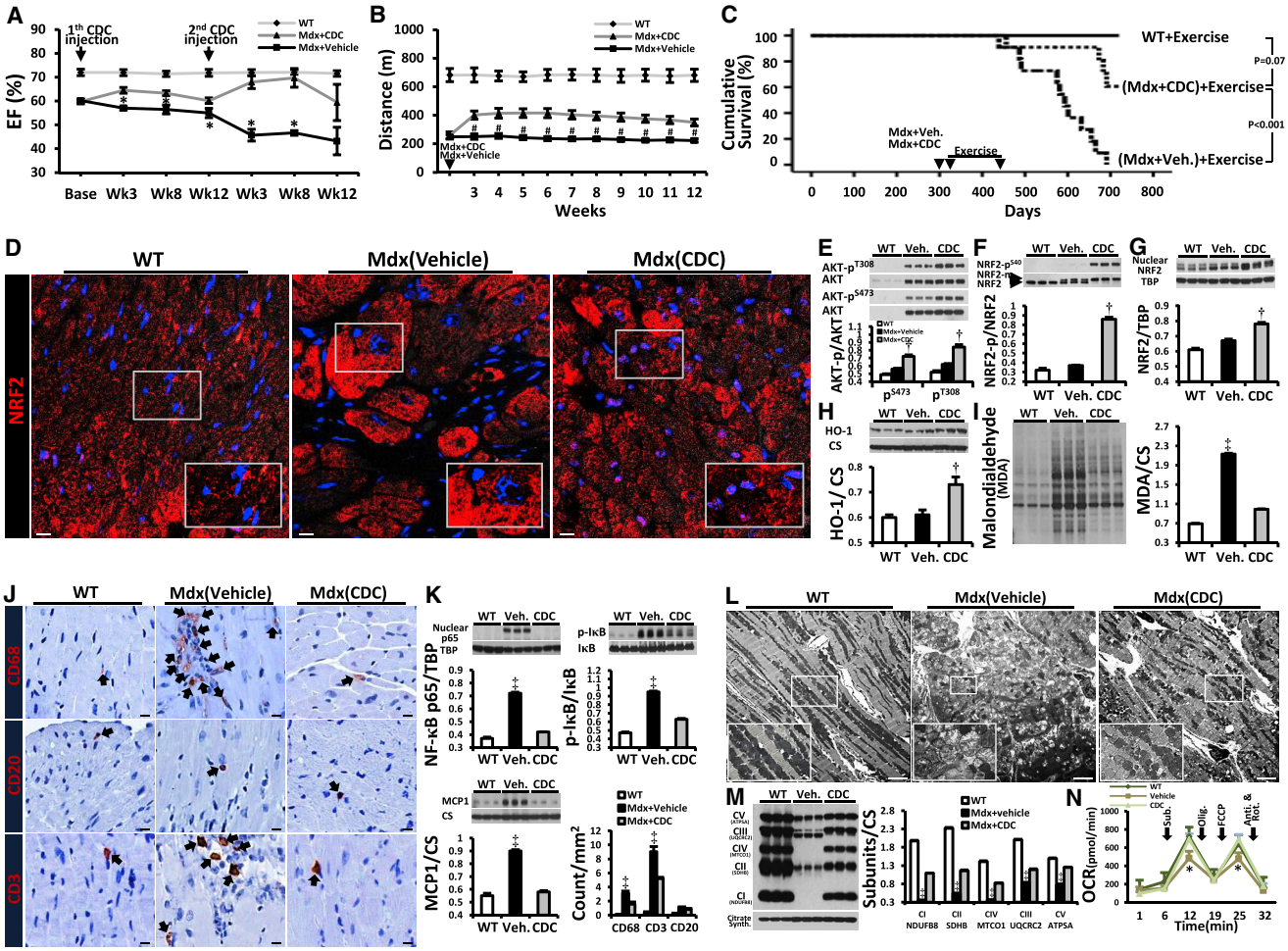

Figure 1. CDC Transplantation into *mdx* Hearts

Function, survival, antioxidant pathways, inflammation, and mitochondrial dysfunction improved by CDC transplantation into *mdx* mice.

(A) Ejection fraction (EF) in CDC-injected *mdx* mice (Mdx + CDC) and vehicle-injected *mdx* mice (Mdx + vehicle) in response to injections at baseline (10 months of age) and 3 months later (WT, n = 7; Mdx + vehicle and Mdx + CDC, n = 12 each).

(B) Exercise capacity in mice subjected to weekly high-intensity treadmill exercise, starting 3 weeks after single-dose CDC or vehicle administration (WT, n = 7; Mdx + vehicle and Mdx + CDC, n = 11 each). Cardiac (A) and treadmill (B) experiments were performed separately on different groups of experimental mice.

(C) Kaplan-Meier analysis of survival in the same animals as (B) shows lower survival in vehicle-treated *mdx* mice than in CDC-treated *mdx* mice or WT controls ($p < 0.001$, log rank test); the latter two groups, however, were statistically comparable.

(D) Immunohistochemical images of NRF2 in *mdx* mouse hearts 3 weeks after administration of vehicle or CDCs. Age-matched WT mice served as control.

(E–I) Western blots and pooled data for protein abundance of phospho-AKT (AKT-p^{T308}, AKT-p^{S473}; E), cytoplasmic phospho-NRF2 (NRF2-p^{S40}; F), nuclear NRF2 (G), NRF2 downstream gene product, hemeoxygenase-1 (HO-1; H), and malondialdehyde protein adducts (I) in *mdx* mouse hearts 3 weeks after administration of vehicle or CDCs (WT, n = 4; Mdx + vehicle and Mdx + CDC, n = 6 each).

(J) Immunohistochemical images of hearts stained for inflammatory cell markers CD68, CD20, and CD3. Black arrows point to $CD68^+$ (upper row), $CD20^+$ (middle row), and $CD3^+$ (lower row) cells.

(K) Western blots, pooled data, and bar graph (lower right) representing protein abundance of nuclear p65, p-IκB (NF-κB pathway), and MCP1 (monocyte chemoattractant protein1) and average number of indicated inflammatory cells and in *mdx* mouse hearts.

(L) Transmission electron microscopy (TEM) images from *mdx* mouse hearts 3 weeks after administration of vehicle (Mdx + vehicle) or CDCs (Mdx + CDC). Age-matched WT mice served as control.

(M and N) Representative western blots and pooled data for mitochondrial respiratory chain subunits in WT and vehicle/CDC *mdx* heart tissues (M) and oxygen consumption rate (OCR) of mitochondria isolated from the hearts of WT and CDC- or vehicle-treated

(legend continued on next page)

ventricular function (as manifested by ejection fraction [EF]) and volumes, relative to placebo, for at least 6 months (Figures 1A and S1A). The CDC-induced improvement in EF persisted beyond the point at which no surviving CDCs were detectable in *mdx* hearts (3 weeks after CDC delivery; Figure S1B). In addition to improving EF, CDC injection enhanced ambulatory function (Figure 1B). Ten-month-old wild-type mice (WT) and *mdx* mice (distinct from the *mdx* mice studied in Figure 1A) were subjected to weekly high-intensity treadmill exercise, starting 3 weeks after single-dose CDC or vehicle administration. CDC-treated *mdx* mice showed a substantial increase in maximal exercise capacity, relative to vehicle-treated *mdx* mice, over the 3 months that exercise capacity was measured; survival also differed in the two groups (Figure 1C). By ~23 months of age, all vehicle-treated *mdx* mice had died, whereas >50% of CDC-treated *mdx* mice remained alive (Figure 1C). In investigating the mechanism, we studied known (anti-oxidative, anti-inflammatory, anti-fibrotic, and cardiomyogenic) effects of CDCs (Aminzadeh et al., 2015b; Cheng et al., 2012; Chimenti et al., 2010; Davis et al., 2009; Ibrahim et al., 2014; Lee et al., 2011; Li et al., 2010; Makkar et al., 2012, 2014; Malliaras et al., 2012; Smith et al., 2007; Tseliou et al., 2013; White et al., 2013). Injection of CDCs led to major changes in the expression of genes related to oxidative stress, inflammation, and mitochondrial integrity (Figures S1C–S1G). The NRF2 antioxidant pathway was activated in CDC-treated *mdx* heart (Figure 1D). NRF2 is normally repressed by KEAP1, but oxidative stress (as well as NRF2 phosphorylation by protein kinases such as AKT) causes dissociation of the NRF2-KEAP1 complex, culminating in nuclear translocation of NRF2 and transcriptional activation of antioxidant enzymes (Martin et al., 2004). In *mdx* hearts, levels of phosphorylated AKT (Figure 1E), total NRF2 (Figure 1F), and nuclear NRF2 (Figure 1G) were high (as expected in response to oxidative stress); CDC treatment further increased their protein levels (Figures 1D–1G) and those of downstream gene products (hemeoxygenase-1 [HO-1], catalase, superoxide dismutase-2 [SOD-2], and the catalytic subunit of glutamate-cysteine ligase [GCLC]; Figures 1H and S1G). Concomitantly, oxidative stress was attenuated, as demonstrated by a profound reduction of malondialdehyde adducts (Figure 1I). Histologic analysis revealed extensive fibrosis in vehicle-treated *mdx* hearts, but much less in CDC-treated *mdx* hearts (comparable with an age-matched WT control; Figure S2A). Likewise, CDC treatment largely reversed the accumulation of collagens I and III in *mdx* heart tissue 3 weeks after treatment (Figure S2B). CDCs inhibited the inflammation (Figures 1J and 1K) and mitochondrial dysfunction (Figures 1L–1N) characteristic of *mdx* cardiomyopathy. Nuclear factor κB (NF-κB), the master regulator of pro-inflammatory cytokines and chemokines (Carlson et al., 2005), was activated in vehicle *mdx* hearts (Figure 1K, top panel). Increases in phosphorylated IκB and nuclear p65 were accompanied by upregulation of MCP1 (monocyte chemoattractant protein1) and accumulation of $CD68^+$ macrophages and $CD3^+$ T cells (Figure 1K, bottom panel). CDC treatment reversed activation of NF-κB and decreased the number of inflammatory cells in *mdx* hearts 3 weeks after CDC injection (Figures 1J, 1K, and S2C). Mitochondrial structure and function are abnormal in muscular dystrophy-associated heart failure (Burelle et al., 2010). Whole-transcriptome analysis revealed major changes in the expression of genes related to mitochondrial integrity in *mdx* hearts (Figure S1D). Consistent with this finding, CDCs restored mitochondrial ultrastructure (Figure 1L), increased mtDNA copy numbers (but not mitochondrial number; Figure S3A), augmented levels of respiratory chain subunits (Figure 1M), and normalized the deficient respiratory capacity of isolated *mdx* mitochondria (Figure 1N). Of note, the salutary mitochondrial changes were associated with upregulation of antioxidant enzymes and reductions of oxidative stress and inflammation (Figures 1D–1K, S1E–S1G, and S5). We also probed the effects of CDCs on cardiomyogenesis. Vehicle-treated *mdx* hearts exhibited a modest increase in the numbers of cycling ($Ki67^+$) and proliferating (aurora B^+) cardiomyocytes (Figures S3B and S3C), presumably as a compensation for ongoing cardiomyocyte loss. CDCs are known to increase endogenous cardiomyogenesis in ischemic (Cheng et al., 2012; Lee et al., 2011; Li et al., 2012; Makkar et al., 2012; Malliaras et al., 2014) and non-ischemic models (Aminzadeh et al., 2015b). Similar effects were seen in the *mdx* heart: CDC treatment promoted cardiomyocyte cycling and proliferation, as demonstrated by a marked increase in $Ki67^+$ and aurora B^+ cardiomyocytes (Figures S3B and S3C).

CDC Exosome Transplantation in *mdx* Hearts

CDC exosomes mimic the functional and structural benefits of CDCs in a murine model of myocardial infarction (Ibrahim et al., 2014). In *mdx* mice, likewise, exosomes, isolated from media conditioned by hypoxic CDCs,

mdx mice (N) 3 weeks after treatment (WT, n = 3; Mdx + vehicle and Mdx + CDC, n = 8 each). Substrates (pyruvate, malate, and ADP), a selective uncoupler (FCCP) and blockers (oligomycin [Olig.]; antimycin and rotenone [Anti. & Rot.]) of oxidative phosphorylation were applied when indicated. Pooled data are means ± SEM, CM: cardiomyocyte.

*$p < 0.05$ versus Mdx + CDC; #$p < 0.005$ versus Mdx + CDC; †$p < 0.05$ versus Mdx + Vehicle and WT; ‡$p < 0.002$ versus Mdx + CDC and WT. Scale bars: 10 μm (D and J); 5 μm (L).

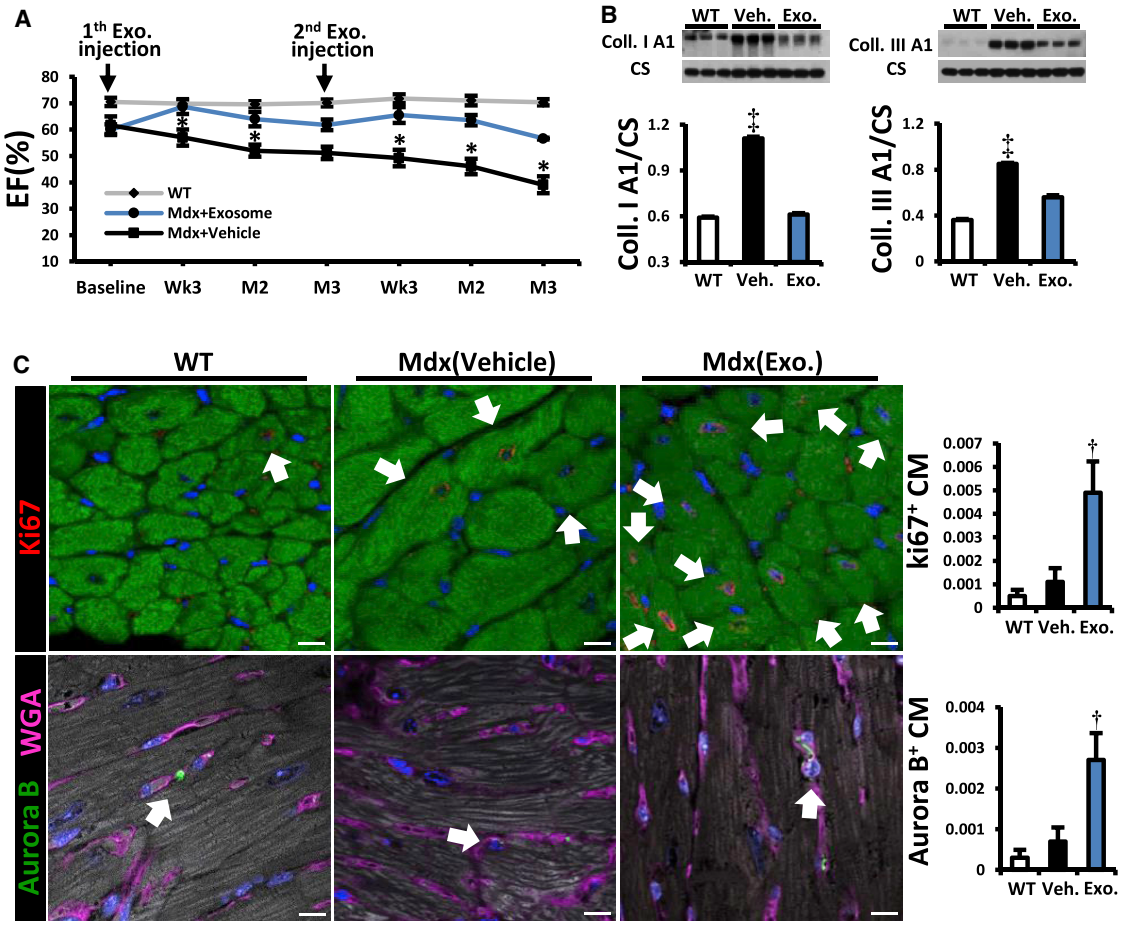

Figure 2. CDC Exosome Injection into *mdx* Hearts Reproduces the Benefits of CDCs

(A) Sustained functional benefit for at least 3 months with each of two sequential CDC exosome injections in *mdx* mice (n = 11).

(B) Western blots and pooled data for cardiac collagen IA and IIIA.

(C) Immunohistochemical images and pooled data (WT, n = 4; vehicle and CDC exosome-treated [Mdx (XO)], n = 6 each) from *mdx* mouse hearts stained for Ki67 [upper row] and Aurora B [lower row]. Arrows point to Ki67$^+$ (upper row) and Aurora B$^+$ (lower row) cardiomyocytes. Data are means ±SEM; *p < 0.05 versus Mdx + exosome; ‡p < 0.01 versus Mdx + exosome and WT; †p < 0.02 versus Mdx + vehicle and WT mice. Scale bar: 10 μm.

reproduced the benefits of CDCs (Figures 2A–2C and S4A–S4D). Two repeat doses of human CDC exosomes (separated by 3 months) led to sustained improvement in EF, relative to vehicle injection (Figures 2A and S4B), with a minimal but detectable humoral response in the non-immunosuppressed *mdx* mice (Figure S4C). Collagen I and III levels decreased (Figure 2B) while cycling (Ki67$^+$, Figure 2C upper row) and proliferating (aurora B$^+$, Figure 2C lower row) cardiomyocytes increased in CDC exosome-injected *mdx* hearts.

Remote Effects of CDC Transplantation in *mdx* Heart

Intramyocardial injection of CDCs and their exosomes improved Duchenne cardiomyopathy, reversing key pathophysiological processes in the *mdx* mouse heart (Figures 1 and 2). These changes were associated with a substantial increase in exercise capacity, which was disproportionate to the improvement in cardiac function: EF increased by <10% (Figure 1A), while ambulatory capacity doubled (Figure 1B). To further evaluate the mechanism of enhanced exercise capacity in CDC-treated *mdx* mice, we isolated and examined three distinct skeletal muscles: the diaphragm (DIA, a key respiratory muscle), and two limb muscles (soleus and extensor digitorum longus [EDL], representative of slow and fast twitch muscles, respectively) 3 weeks after intramyocardial injection of CDCs or vehicle. Whole-transcriptome analysis in DIA revealed downregulation of pathways related to intracellular [Ca^{2+}] excess, oxidative stress, and inflammation after intramyocardial CDC injection (Figures 3A and S5A).

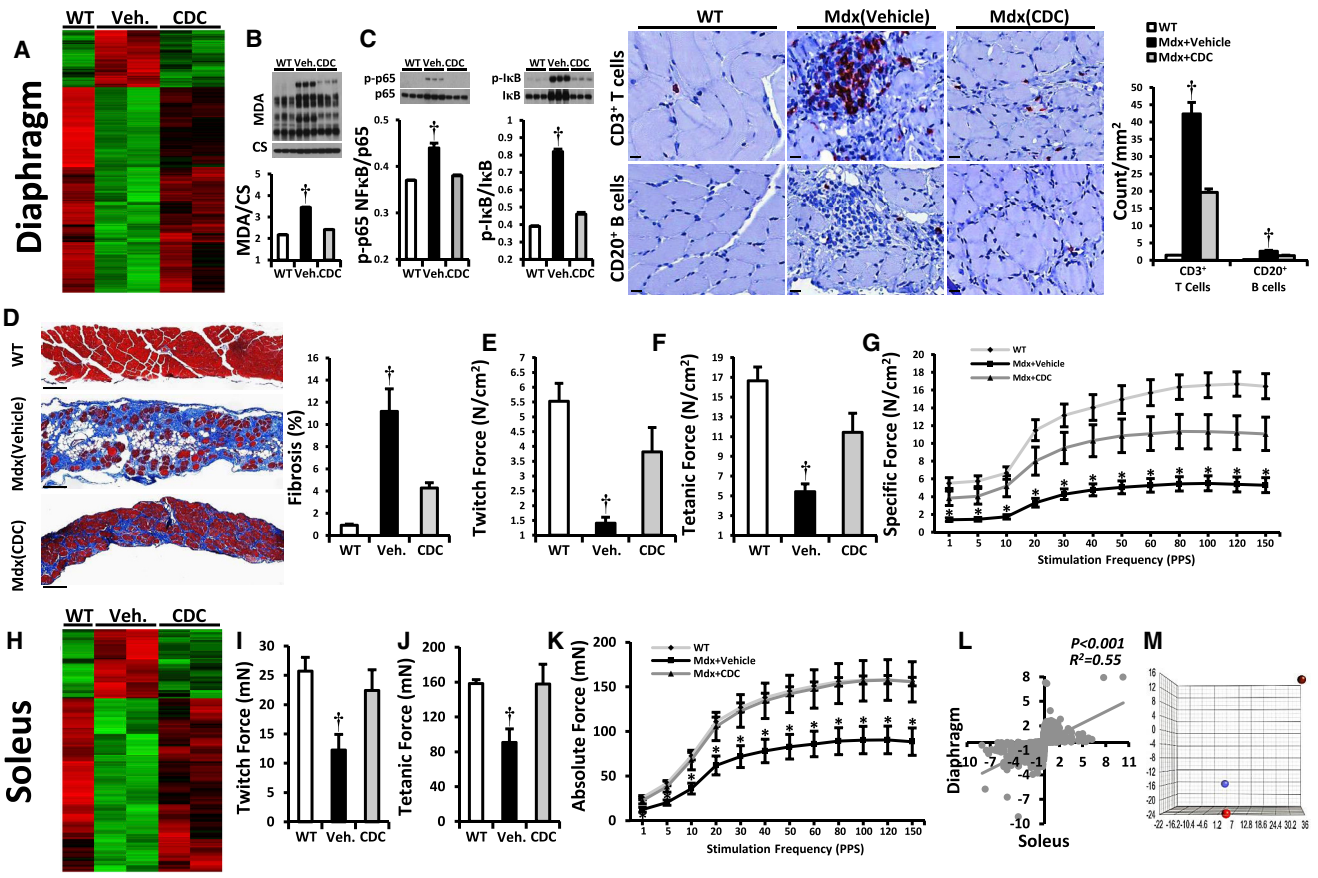

Figure 3. CDC Transplantation in *mdx* Hearts Conferred Beneficial Effects on Diaphragm and Soleus Muscles

(A) Two-dimensional hierarchical clustering using genes with at least two times fold change difference between vehicle/CDC *mdx* diaphragms.

(B and C) Western blots and pooled data for protein abundance of malondialdehyde protein adducts (B), cytoplasmic p-p65 and p-IκB (C; NF-κB pathway; WT, n = 4; vehicle and CDC, n = 6 each) and immunohistochemical images of diaphragm stained for inflammatory cell markers CD20 and CD3; bar graph represents the average number of indicated inflammatory cells 3 weeks after administration of vehicle or CDCs into *mdx* hearts.

(D) Representative Masson trichrome images and morphometric analysis in diaphragms 3 weeks after administration of vehicle or CDCs into the hearts of *mdx* mice.

(E–G) *In vitro* measurement of isometric diaphragm contractile properties: twitch force (E), maximum tetanic force (F), and force/frequency relationships (G) 3 weeks after CDC/vehicle *mdx* heart treatments.

(H) Two-dimensional hierarchical clustering using genes with at least two times fold change difference between vehicle/CDC *mdx* soleus.

(I–K) *In vitro* measurement of isometric soleus contractile properties: twitch force (I), maximum tetanic force (J), and force/frequency relationships (K) 3 weeks after CDC/vehicle treatment of *mdx* hearts.

(L) Correlation of fold changes in expression of same genes in diaphragm and soleus 3 weeks after intramyocardial CDC injection in *mdx* mice.

(M) Three-dimensional plot depicting principal components analysis (PCA) of RNA-seq expression data from exosomes isolated from hypoxic conditioned media and effluents of CDC- or vehicle-treated *mdx* hearts. The effluent of isolated *mdx* hearts undergoing Langendorff perfusion was collected for exosome isolation and subsequent RNA-seq 3 days after intramyocardial CDC/vehicle injection. PCA analysis showed clustering of CDC exosomes (red) with exosomes isolated from effluent of CDC *mdx* hearts (blue), but not vehicle-injected *mdx* hearts (stippled), indicating that CDC exosomes were shed from *mdx* hearts at least 3 days after intramyocardial CDC injection. Effluents of *mdx* hearts from the same group were pooled (n = 3 for each group).

Data are means ±SEM; *p < 0.05 versus Mdx + CDC; †p < 0.05 versus Mdx + CDC and WT mice. Scale bars: 10 μm (C); 100 μm (D).

Decreases in malondialdehyde protein adducts (Figure 3B), repressed NF-κB, reduced infiltration of inflammatory cells (Figure 3C), and diminished fibrosis (Figure 3D) paralleled a marked improvement in the contractile function of DIA (Figures 3E–3G). Similarly, soleus (Figures 3H–3K) and EDL (Figures S5B–S5D) showed notable improvements at

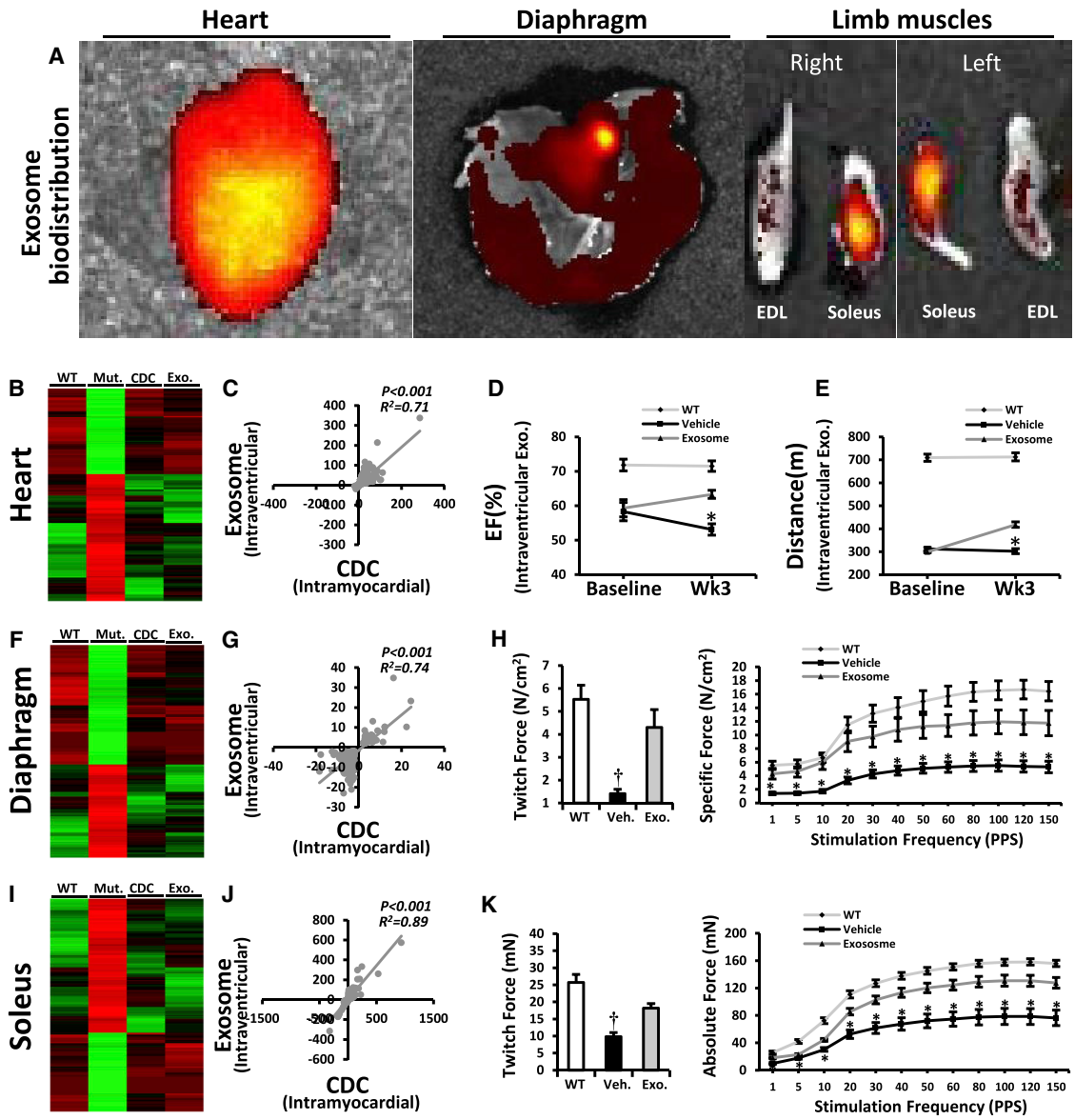

Figure 4. Systemic CDC Exosome Injection Mimicked the Cardiac and the Remote Effects of Intramyocardial CDC Injection in *mdx* Mice

(A) Systemic biodistribution of CDC exosomes after intraventricular injection in *mdx* mice. CDC exosomes were stained with fluorescent lipid dye and tracked 6 hr later using bioluminescence imaging.

(B) Two-dimensional hierarchical clustering using genes from hearts of non-treated *mdx* mice and of *mdx* mice treated intramyocardially with CDCs or intraventricularly with CDC exosomes. Genes with at least 2-fold differences with corresponding transcripts in non-treated *mdx* mice were included.

(C) Correlation of fold changes in expression of same genes 3 weeks after intramyocardial CDC injection or intraventricular CDC exosome injection in *mdx* hearts.

(D and E) EF and exercise capacity in *mdx* mice 3 weeks after intraventricular injection of vehicle/CDC exosome (WT, n = 5; Mdx + vehicle and Mdx + CDC exosome, n = 9 each).

(F) Two-dimensional hierarchical clustering using genes from diaphragm of non-treated *mdx* mice and of *mdx* mice treated intramyocardially with CDCs or intraventricularly with CDC exosomes. Genes with at least 2-fold differences with corresponding genes in non-treated *mdx* mice were included.

(G) Correlation of fold changes in expression of the same genes in diaphragm 3 weeks after intramyocardial CDC injection or intraventricular CDC exosomes injection.

(legend continued on next page)

transcriptomic, histologic, and functional levels; soleus fibrosis (Figure S5D) was attenuated and contractile force (Figures 3I–3K) was augmented. Changes in gene expression in DIA and soleus were significantly correlated (Figure 3L).

As a basis for the remote effects of intramyocardial injection of CDCs on skeletal muscle, we considered the possibility that exosomes secreted by CDCs lodged in the heart might exit in the venous effluent and exert remote signaling. Principal components analysis revealed that CDC exosomes were very similar in their RNA content to the exosomes isolated from effluents of isolated CDC-treated *mdx* hearts, but quite distinct from exosomes in the effluents of vehicle-treated *mdx* hearts 3 days after intramyocardial CDC injection (Figure 3M), pinpointing exosomes as likely mediators of the secondary systemic effects. Such secondary effects are extensive: whole-transcriptome analysis of liver (Figure S6A) 3 weeks after intramyocardial CDC injection revealed downregulation of inflammatory pathways in liver analogous to what we found in heart and skeletal muscle. Thus, CDCs' secondary effects are not restricted to muscle.

Systemic CDC Exosome Injection

To further evaluate the potential of exosomes to mediate systemic benefits, we injected CDC exosomes into the left ventricular cavity of *mdx* hearts. Six hours post injection, fluorescently labeled CDC exosomes were evident not only in the heart and skeletal muscle (Figure 4A) but also in brain, liver, lung, spleen, gut, and kidneys (Figure S6B). Changes in *mdx* heart (Figures 4B–4E), diaphragm (DIA; Figures 4F–4H), and soleus (Figures 4I–4K) 3 weeks after intraventricular CDC exosome injection mimicked the modifications seen in these organs after intramyocardial CDC injection (Figure 3). Taken together, the results in Figures 1, 2, 3, and 4 implicate CDC exosomes as mediators of the local and remote effects of intramyocardial CDC injection.

CDC Exosome Injection into *mdx* Skeletal Muscle

To investigate primary effects on skeletal muscle, we injected CDC exosomes directly into the soleus in *mdx* mice. Histologic analysis revealed a paucity of surviving myofibers in vehicle-injected *mdx* soleus relative to WT controls, and those that remained were hypertrophic (Figure 5A). CDC exosomes markedly increased the total number of myofibers and shifted the size distribution to smaller diameters, indicative of myofiber proliferation 3 weeks after injection (Figure 5B). Consistent with this interpretation, the number of $MYOD^+$ cells was augmented after CDC exosome injection (Figures 5A and 5C), with increased tissue levels of MYOD and myogenin, the major transcription factors orchestrating myoblast determination and differentiation, respectively (Bentzinger et al., 2012) (Figure 5D). In physiologic muscle growth, insulin growth factor (IGF)-1 is commonly implicated as an upstream signal (Schiaffino and Mammucari, 2011), but the effects of CDC exosomes on *mdx* soleus muscle were independent of IGF-1 receptors (Figure 5E). Along with enhanced muscle regeneration, intrasoleus CDC exosome injection decreased inflammation (Figure 5F) and fibrosis (Figure 5G). The net effect was complete restoration of contractile force in soleus muscles injected with CDC exosomes (Figure 5H).

CDC Exosomes in Human Duchenne Cardiomyocytes Derived from iPSCs

Demonstration of efficacy in multiple models of DMD would bolster the notion that CDC exosomes may be viable therapeutic candidates. Duchenne human induced pluripotent stem cell (iPSC)-derived cardiomyocytes (DMD CMs) exhibit a number of phenotypic deficits characteristic of DMD, including decreased oxygen consumption rate (OCR) reminiscent of that observed in *mdx* heart mitochondria (Figure 1N), and abnormal calcium cycling (Guan et al., 2014). Priming DMD CMs with CDC exosomes 1 week earlier suppressed beat-to-beat calcium transient alternans during 1 Hz burst pacing (a measure of arrhythmogenicity; Clusin, 2008) (Figure 6A) and normalized OCR (Figure 6B). The congruence of experimental findings in the two DMD models is noteworthy: the *mdx* mouse has a nonsense mutation in exon 23 of the murine dystrophin gene leading to a premature termination codon (PTC), while the DMD patient whose iPSCs were studied here has a fundamentally different genetic lesion in the human dystrophin gene (exon 50 deletion with frameshift; Guan et al., 2014). Thus, CDC exosomes exert salutary effects in at least two classes of DMD mutations.

Dystrophin Expression after Injection of CDCs or Their Exosomes in *mdx* Mice

In assessing the seemingly unlikely possibility that CDCs and/or CDC exosomes might restore expression of dystrophin, we were surprised to contradict our preconception. Figure 7 shows immunohistochemical images (Figure 7A) and immunoblots (Figures 7B–7D) demonstrating partial,

(H) Diaphragm isometric twitch force and force/frequency relationships 3 weeks after intraventricular CDC exosome injection.
(I–K) Two-dimensional hierarchical clustering (I), correlation analysis (J), and isometric twitch force and force/frequency relationships (K) from soleus muscle 3 weeks after intraventricular CDC exosome injection.
Data are means ± SEM; *$p < 0.05$ versus Mdx + CDC exosome; $^{\dagger}p < 0.05$ versus Mdx + CDC exosome and WT mice.

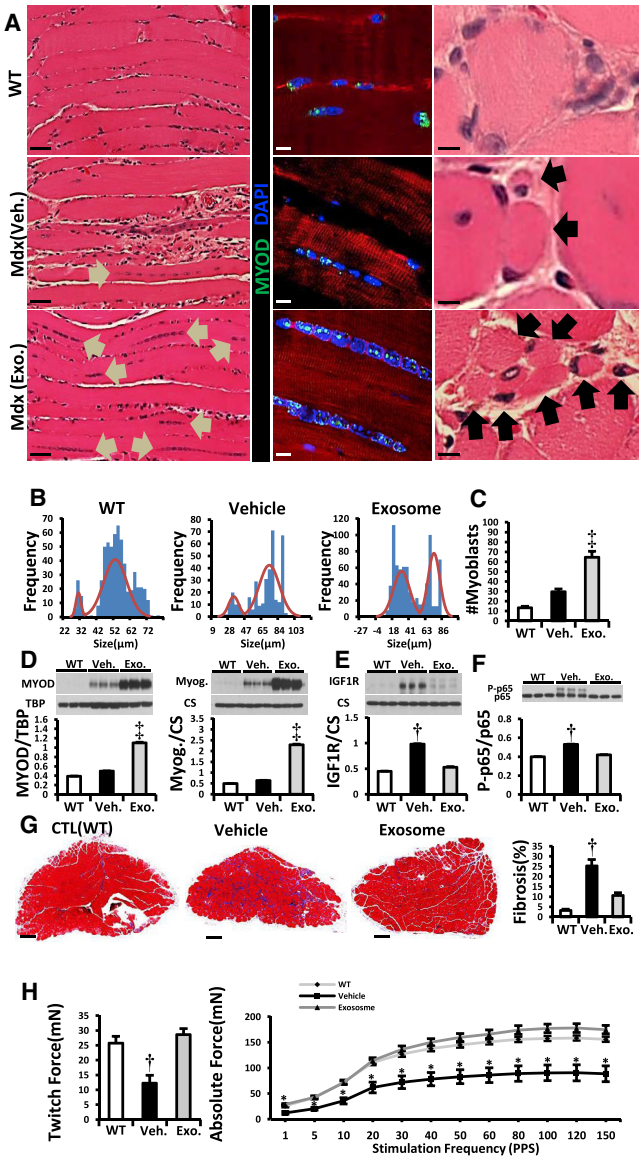

Figure 5. Intramuscular Injection of CDC Exosomes Resulted in Muscle Growth and Reversal of Pathophysiologic Abnormalities

(A) H&E and immunohistochemical images of soleus muscle stained for MYOD (WT, vehicle, and CDC exosome-treated [*Mdx* (exosome)] *mdx* mouse soleus). Arrows in H&E images point to the lined-up nuclei (left column) and myofibers (right column). In the immunohistochemistry, linearly arranged nuclei were positive for MYOD (middle column).

(B and C) Frequency distribution of myofiber sizes and number of myoblasts ($MYOD^+$) 3 weeks after vehicle/CDC exosome injection in *mdx* soleus muscles (WT, n = 5; vehicle and exosome, n = 9 each).

(D–F) Western blots and pooled data for protein abundance of MYOD, myogenin (D), IGF1 receptor (IGF1R; E) and cytoplasmic p-p65 (F) in *mdx* soleus muscles 3 weeks after intrasoleus vehicle/CDC exosome injection (WT, n = 4; vehicle and exosome, n = 6 each).

transient dystrophin expression after injection of CDCs (Figures 7A and 7B) or exosomes (Figures 7C and 7D). Three weeks after intramyocardial injection of CDCs, immunohistochemistry of heart (Figure 7A, left), diaphragm (center) and soleus (right) revealed apparent restoration of dystrophin expression, with appropriate membrane localization, to all these muscles. While immunohistochemical images can be difficult to interpret quantitatively (van Putten et al., 2013), western blots of CDC-injected hearts (Figure 7B) reveal the re-expression of full-length dystrophin (427 kDa) to be relatively low ($\leq$10% of WT levels 3 weeks post injection), and transient (no detectable bands 3 months post injection). Interestingly, partial restoration of dystrophin was also evident after intramyocardial injection of CDC exosomes (Figure 7C). Consistent with the transient nature of dystrophin re-expression after CDC injection (Figure 7B), CDC exosomes led to visible dystrophin bands in the heart 1 and 3 weeks, but not 3 months, after systemic injection (Figure S6C). Among various tissues collected and analyzed 1 week after systemic exosome delivery (Figure 7D), detectable levels of dystrophin were evident in heart, diaphragm, and soleus but not in tibialis anterior and EDL muscles or in the hypothalamus. Thus, CDCs and their exosomes induce measurable dystrophin re-expression in heart and certain types of skeletal muscle, but the effect is transient.

Many, if not most, of the effects of exosomes are attributable to their RNA and protein payloads (Vyas and Dhawan, 2016). In CDC exosomes, dystrophin protein was undetectable (Figure S6D), and dystrophin transcripts were absent by RNA sequencing (RNA-seq) and undetectable by qPCR (Figure S6D), so dystrophin restoration is not due to exosomally mediated transfer of its protein or mRNA. Nevertheless, regulatory RNA may act directly or indirectly to increase dystrophin expression, e.g., by read-through of PTCs (Advani and Dinman, 2016). RNA-seq of CDC exosomes grown under our conditions revealed 144-fold augmentation of miRNA 148a (*Mir-148a*; Figure S6E), which we tested as a candidate effector. Intramyocardial injection of *Mir-148a* restored expression of dystrophin in *mdx* hearts 3 weeks after administration (Figure 7E).

(G) Representative Masson trichrome images and morphometric analysis in *mdx* soleus muscles 3 weeks after administration of vehicle or CDC exosomes into *mdx* soleus (WT, n = 5; vehicle and exosome. n = 9 each).

(H) *In vitro* measurement of soleus isometric twitch force and force/frequency relationships 3 weeks after vehicle/CDC exosome injection into *mdx* soleus muscles.

Pooled data are means ± SEM. *$p < 0.05$ versus Mdx + CDC exosome; $^{\dagger}p < 0.05$ versus Mdx + CDC exosome and WT mice; $^{\ddagger}p < 0.002$ versus Mdx + vehicle and WT mice. Scale bars: 5 μm (A, right column), 10 μm (A, middle column), 50 μm (A, left column), and 200 μm (G).

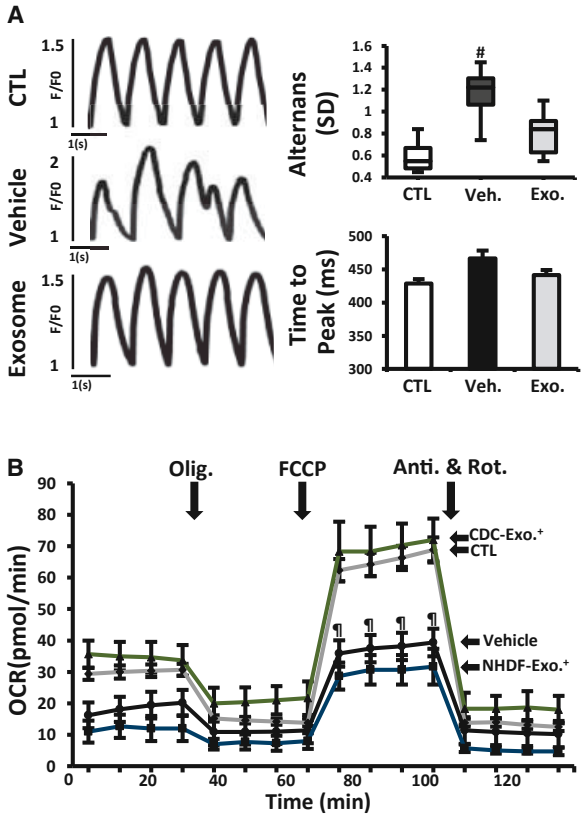

Figure 6. CDC Exosomes in Human Duchenne Cardiomyocytes Derived from iPSCs

(A) Calcium transients from normal and DMD CM measured during 1 Hz burst pacing. Duchenne cardiomyocytes were primed with vehicle or CDC exosomes (exosomes) 1 week before assessment. Bar graphs of calcium transient alternans (variation in beat-to beat calcium transient amplitude) and time to peak (n = 10 cells in each group).

(B) Oxygen consumption rate (OCR) in DMD CMs primed with CDC exosomes or exosomes from normal human dermal fibroblasts (NHDF, as control; NHDF exosome) 1 week before OCR measurement. Normal (CTL) and non-treated DMD CM (vehicle) were studied in parallel. Results from four independent experiments performed in three replicates are shown. See Figure 1 legend for abbreviations. All data are means ± SEM except for the boxplot (means ± SD).

$^{\#}p < 0.03$ versus CDC exosome and CTL (normal cardiomyocyte); $^{\P}p < 0.02$ versus CDC exosome.

Like CDC exosomes, *Mir-148a* (but not a scrambled miRNA) increased EF in *mdx* mice (Figure 7F). The unexpected bioactivity of *Mir-148a* on dystrophin occurred in parallel to suppression of known *Mir-148a* targets (NF-κB p65 and phospho-AKT; Bao and Lin, 2014) (Figures 7G and 7H). Analysis of exon-intron junctions for dystrophin transcripts in *mdx* hearts exposed to CDCs, CDC exosomes, or *Mir-148a*, shows no treatment-related exon skipping or alternative splicing (Figure S7A). Thus, we have excluded exosomal dystrophin mRNA or protein transfer, as well as RNA splicing, while implicating *Mir-148a* as a potential mediator of enhanced full-length dystrophin protein synthesis.

DISCUSSION

We propose that CDCs act by secreting exosomes, which are taken up by surrounding myocardium and by distant skeletal muscle, antagonizing multiple pathophysiological pathways active in DMD. The congruent effects in *mdx* mice (Figures 1, 2, 3, 4, and 5) and in exon 50-deleted DMD hCM (Figure 6) highlight the ability of CDC exosomes to benefit multiple disease-causing dystrophin mutations. We found, unexpectedly, that CDCs and their exosomes increase dystrophin expression in the *mdx* mouse model. Various lines of evidence exclude alternative splicing, mRNA, or protein transfer, supporting the idea that translational readthrough enhances dystrophin expression in the exon 23 PTC *mdx* mutant, perhaps by exosomally mediated transfer of *Mir-148a*. Additional work will be required to pinpoint the precise mechanism of enhanced dystrophin expression and to determine if the effect is generalizable to other types of DMD mutations. Nevertheless, the dystrophin-independent actions of CDCs and their exosomal contents should be generalizable. After all, CDCs and their exosomes work quite well in cardiomyopathies not associated with dystrophin deficiency (Aminzadeh et al., 2015b; Gallet et al., 2017; Ibrahim et al., 2014). The protean actions of CDCs and their exosomes include improved mitochondrial function, enhanced myocyte proliferation, and suppression of oxidative stress, inflammation, and fibrosis (Figure 7). Observed effects, which must be independent of dystrophin restoration, include the suppression of inflammation in *mdx* liver (an organ with no dystrophin expression; Love et al., 1991) as well as the persistent benefits in heart 3 months after injection of CDCs or CDC exosomes (at which time dystrophin is no longer detectable). Notably, CDCs and their exosomes not only reverse the dystrophic phenotype but also forestall disease progression: the functional benefits of cardiac injections of CDCs or their exosomes persist for at least 3 months, and single doses of CDCs decrease mortality more than 1 year later in *mdx* mice. These findings beg the investigation of exosomally triggered epigenomic modifications as a potential basis for the durable benefits (Lee et al., 2012), but such experiments are beyond the scope of this report.

The HOPE-Duchenne trial was designed to assess single-dose delivery of CDCs to the heart (Ascheim and Jefferies, 2016). Exploratory efficacy data reported recently from this 25-patient randomized trial give credence to the idea that CDCs may benefit not only the cardiomyopathy but

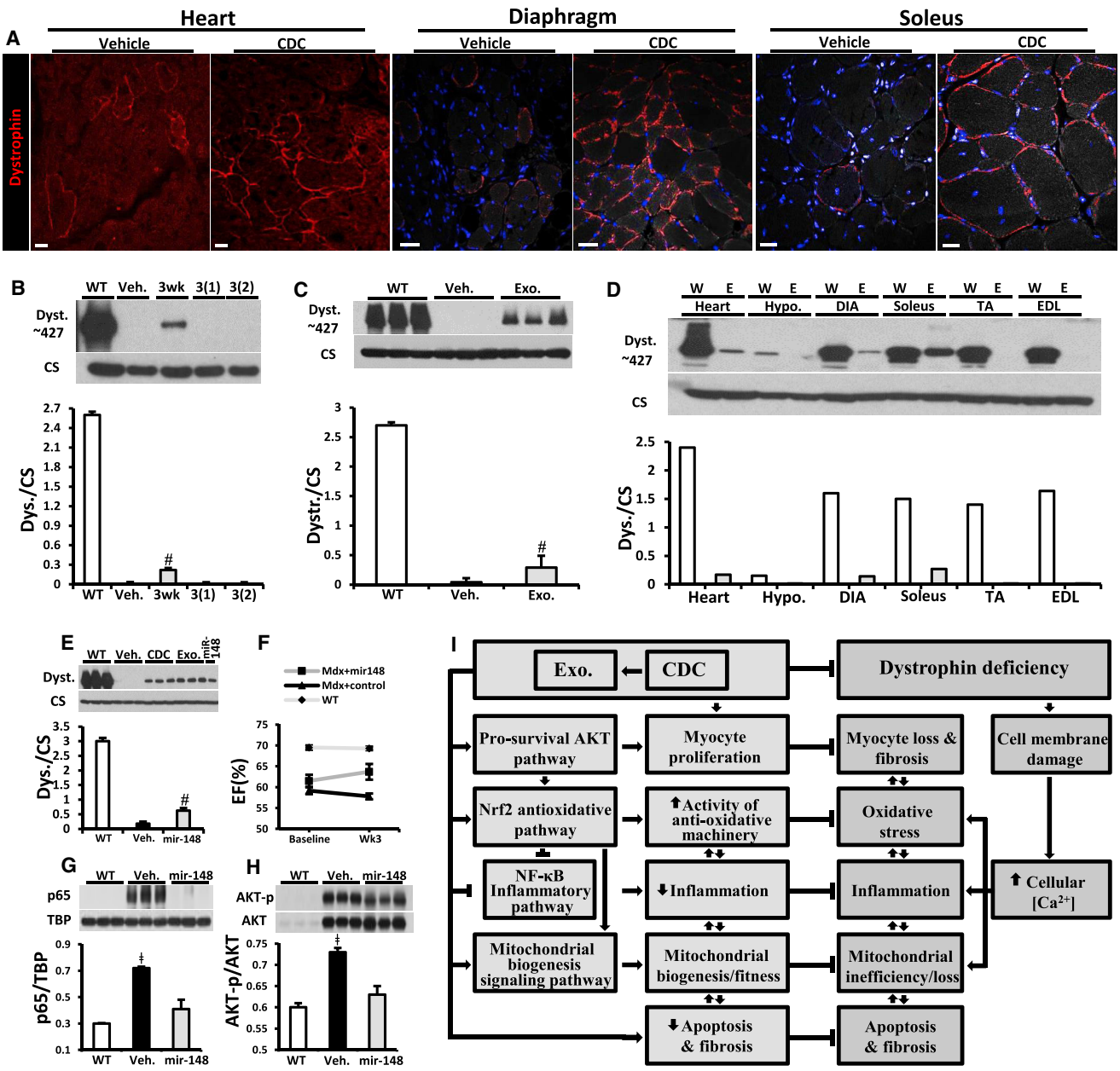

Figure 7. Exosomes Mediate Reversal of Key Pathophysiological Features of Duchenne Muscular Dystrophy

(A) Immunohistochemical images of dystrophin in *mdx* mouse heart, diaphragm, and soleus treated with and without CDC at 10 months of age.

(B) Western blot and pooled data for dystrophin protein in WT control mouse heart and *mdx* mouse hearts 3 weeks and 3 months after first intramyocardial CDC injection, 3(1), and 3 months after second (repeat) CDC injection into myocardium, 3(2), versus Mdx + vehicle (Veh.); (Mdx + vehicle and Mdx + CDC, n = 6 each).

(C) Western blot and pooled data for dystrophin protein in WT control mouse heart and *mdx* mouse hearts 3 weeks after CDC exosome injection into myocardium (Mdx + vehicle and Mdx + exo, n = 6 each).

(D) Western blot showing protein content of dystrophin in WT control and in *mdx* mouse (Exo) heart, hypothalamus (hypo.), diaphragm (DIA), soleus, tibialis anterior (TA), and extensor digitorum longus (EDL) 1 week after systemic CDC exosome delivery by intraventricular injection (n = 2).

(E) Western blots and pooled data for protein abundance of dystrophin isoform: dp427 in *mdx* mouse hearts 3 weeks after intramyocardial injection of vehicle, CDC, CDC exosomes, or mimics of *Mir-148a*.

(legend continued on next page)

also the skeletal myopathy of DMD (Jefferies et al., 2017). A follow-on placebo-controlled trial of CDCs in DMD patients, HOPE-2, is currently being planned (Kegel, 2017). Given the preclinical insights reported here and elsewhere (Rogers et al., 2017), CDCs will be administered systemically in HOPE-2, thereby avoiding the need for cardiac catheterization.

In addition to CDCs themselves, exosomes derived from CDCs are promising next-generation therapeutic candidates (TCs). Although CDCs and their exosomes exert multiple, synergistic benefits (Figure 7I), focused dystrophin augmentation, even if at much lower levels than normal (van Putten et al., 2013), may be no less valuable a concept to pursue. CDC-exosomes carry all the instructions required to induce dystrophin re-expression, and clinical-grade manufacturing is feasible (Marbán, 2018). Nevertheless, a defined agent would have considerable reductionist appeal. Emergent insights pinpoint *Mir-148a* as a defined agent that increases dystrophin expression, making it a promising third-generation TC. The dystrophin-enhancing effects of CDC exosomes, and presumably of *Mir-148a*, wear off between 3 weeks and 3 months, but repeated delivery of either agent (~monthly) may lead to sustained dystrophin enhancement; however, we have not yet tested this conjecture. All three TCs (CDCs, CDC exosomes, and *Mir-148a*) have mechanisms of action complementary to, and potentially synergistic with, those of the approved exon-skipping agent etiplirsen, or of other treatment approaches currently in active development for DMD (e.g., myoediting).

EXPERIMENTAL PROCEDURES

Please see Supplemental Information for expanded methods.

Animal Study

We studied the *mdx* mouse model of DMD (C57BL/10ScSn-Dmdmdx/J) and WT strain-matched mice (C57BL/10ScSnJ WT mouse heart) (Jackson Laboratory, USA) from 10 months of age. All mice studied were female. To optimize the process of CDC transplantation, preliminary dose-response experiments were performed, which identified 1×10^5 cells in the first injection and 1×10^4 cells in the second injection (3 months after the first injection) as effective doses, consistent with prior dose-ranging experiments in ischemic and non-ischemic mouse models (Aminzadeh et al., 2015b; Shen et al., 2012). A total of 1×10^5 cells/40 μL of PBS (first injection) or 1×10^4 cells/40 μL of PBS (second injection) or PBS alone were injected into left ventricular (LV) myocardium divided equally among four sites as described (Aminzadeh et al., 2015b; Nagaya et al., 2005). The LV was visually divided into three zones: basal, middle, and apical, with one injection in the basal, two in the middle, and one in the apical zone. Ten-month-old CDC/*mdx* and vehicle/*mdx* mice were injected with CDCs (Mdx + CDC, n = 12) or vehicle (placebo: Mdx + vehicle [PBS], n = 12) twice (3 month interval), respectively. Injections were during open-chest thoracotomy via a 28.5 gauge needle. All surgical procedures were carried out while the animals were under general anesthesia (dexmedetomidine 0.5 mg/kg/ketamine 75 mg/kg; intraperitoneally; once before surgery). Similar protocols were used for injection of CDC exosomes into myocardium. Intraventricular single injection of CDC exosomes, $(10.32 \pm 3.28) \times 10^9$/150 μL of PBS, or PBS alone into the LV cavity were performed during open-chest thoracotomy via a 28.5 gauge needle. Intramuscular injection of exosomes into soleus (SOL) muscles were performed at a single site at the lower 1/3 of the muscle using a 25 μL Hamilton syringe (with 0.5 μL marks) with a 31 gauge needle. The needle was advanced up to the upper 1/3 of the muscle and then slowly retracted through the belly as exosomes, $(20.64 \pm 2.12) \times 10^7$/3 μL, were injected. Among all mice studied, there was only one perioperative death. To ensure ethical and humane treatment of animals, we adhered to the principles recommended in the Guide for Care and Use of Laboratory Animals with oversight and approval by the Cedars-Sinai Health System Institutional Animal Care and Use Committee and the Department of Comparative Medicine (IACUC#3809).

CDCs, CDC Exosomes, NHDF Exosomes

CDCs

Mouse CDCs were expanded from female WT strain-matched mouse hearts (C57BL/10ScSnJ) as described (Smith et al., 2007). Briefly, ventricular tissues were minced into ~1 mm explants, partially digested enzymatically and plated on adherent (fibronectin-coated) culture dishes. These explants spontaneously yield outgrowth cells (explant-derived cells), which were harvested once confluent and plated in suspension culture (10^5 cells/mL on poly-D-lysine-coated dishes) to enable self-assembly of three-dimensional cardiospheres. Subsequent replating of cardiospheres on adherent culture dishes yielded CDCs, which were used in all experiments at passage one.

CDC Exosomes

Exosomes were isolated from serum-free media conditioned overnight (24 hr) by cultured human male CDCs from two

(F) Ejection fraction (EF) at baseline and 3 weeks after intramyocardial injection of *Mir-148a* or miRNA control in *mdx* mice. WT EF values are also shown for reference, n = 5 per group.
(G and H) Western blots and pooled data for nuclear p65 (G) and phosphorylated AKT (H) in *mdx* mouse hearts 3 weeks after *Mir-148a* treatment (vehicle and *Mir-148a*, n = 6 each).
(I) Schematic of pathophysiological mechanisms operative in Duchenne cardiomyopathy and the cellular mechanisms recruited by CDCs and their exosomes. All organs were from mice 10 months old at baseline.
All data are means ± SEM. $^{\#}p < 0.05$ versus Mdx + vehicle and WT; $^{\ddagger}p < 0.05$ versus Mir-148a and WT. Scale bars: 25 μm (A, heart); 25 μm (A, diaphragm); 20 μm (A, soleus).

different cell lines (Gallet et al., 2017; Ibrahim et al., 2014) (CDC exosome) (or normal human dermal fibroblasts [NHDF] as a control) in hypoxia (2% O_2; default condition) or normoxia (20% O_2, solely for studies comparing RNA content of exosomes). Exosomes from both cell lines, either frozen and thawed or prepared fresh, yielded similar results. Ultracentrifugation (100,000 × *g* for 1 hr) was used to isolate exosomes from conditioned media after sequential centrifugations at 300 × *g* (10 min) and 10,000 × *g* (30 min) and filtration with 0.22 μm filters (Lässer et al., 2012). Isolated exosomes were re-suspended in PBS (for *in vivo* and *in vitro* experiments) and the ratio of exosome to protein was measured using a Nanosight particle counter (Webber and Clayton, 2013) and Micro BCA Protein Assay Kit (Life Technologies, Grand Island, NY), respectively. Preliminary dose-response studies identified (2.24 ± 1.34) × 10^7 and (6.19 ± 3.68) × 10^8 exosomes from hypoxic CDCs as effective doses for *in vitro* and *in vivo* (intramyocardial CDC exosome injection) experiments, respectively. Exosomes were characterized by the most rigorous of criteria (Lötvall et al., 2014): linear iodixanol density gradient, transmission electron microscopy (TEM), key membrane proteins, and the biological effect. TEM images of sequentially centrifuged exosomes with and without purification with a linear iodixanol density gradient are shown (Figure S7B). The vesicles are variable in size and morphology, consistent with previous work (Zabeo et al., 2016). Western blots on lysed exosomes showed key proteins characteristic of exosomes: CD63, CD81, and TSG (Figure S7C). Biological activity of sequentially centrifuged exosomes with (Exo1) and without (Exo2) purification with linear iodixanol density were compared by injection into *mdx* soleus muscles and evaluation of *mdx* soleus transcriptome 3 weeks after injection (Figure S7D). Correlation of fold changes in expression of the same genes 3 weeks after Exo1 and Exo2 injection in *mdx* soleus muscles (Figure S7E) demonstrated similar effects of Exo1 and Exo2 and supported the notion that the bioactivity of the vesicles isolated by our default protocol is genuinely due to exosomes and not to another type of vesicles that might have been co-purified by ultracentrifugation.

iPSC-Derived Cardiomyocytes

Urine-derived cells were collected and used as source material for iPSCs, from a male subject with genetically confirmed DMD (exon 50 deletion), and an unaffected control subject, as described (Guan et al., 2014). iPSCs were differentiated to cardiomyocytes following an established protocol with modifications. Briefly, iPSC colonies were detached by 10 min incubation with Versene (Life Technologies, Carlsbad, CA), triturated to a single-cell suspension, and seeded onto Matrigel-coated plastic dishes at a density of 250,000 cells/cm^2 in mTeSR1 medium and cultured for 4 more days. Differentiation was then initiated by switching the medium to RPMI 1640 medium supplemented with 2% insulin-reduced B27 (Life Technologies) and fresh L-glutamine.

SUPPLEMENTAL INFORMATION

Supplemental Information includes Supplemental Experimental Procedures and seven figures and can be found with this article online at https://doi.org/10.1016/j.stemcr.2018.01.023.

AUTHOR CONTRIBUTIONS

M.A.A. designed and performed *in vivo* experiments and data analysis; manufactured exosomes; performed western blots; and wrote first draft of the paper. R.G.R. performed *in vivo* experiments and data analysis; manufactured exosomes; and performed western blots. M.F. performed and analyzed isolated skeletal muscle experiments. R.E.T. assisted with experiments and data analysis. X.G. and M.K.C. prepared and provided cardiomyocytes differentiated from human induced pluripotent cells and performed respirometry experiments on cardiomyocytes differentiated from human induced pluripotent cells. A.M.A., D.J.T., and R.A.G. performed and analyzed respirometry on isolated mitochondria. A.I., R.A.V., and M.L. assisted with experimental design, data analysis, and manuscript drafting. X.D. performed RNA sequencing and analyzed data. A.T. and J.M.G. measured calcium transients in cardiomyocytes differentiated from human induced pluripotent cells and analyzed data. E.M. was responsible for experimental design, data analysis, and preparation of the final manuscript.

ACKNOWLEDGMENTS

This work was supported by grants from Coalition Duchenne and the NIH (R01 HL124074). We thank Liang Li for skilled technical assistance. E.M. is a founder of Capricor and a member of its scientific advisory board. A.I. consults for Capricor.

Received: December 14, 2017
Revised: January 20, 2018
Accepted: January 22, 2018
Published: February 22, 2018

REFERENCES

Advani, V.M., and Dinman, J.D. (2016). Reprogramming the genetic code: the emerging role of ribosomal frameshifting in regulating cellular gene expression. Bioessays *38*, 21–26.

Aminzadeh, M.A., Tobin, R., Smith, R., Marban, L., and Marban, E. (2014). Heart-derived cell therapy for Duchenne cardiomyopathy: cardiosphere-derived cells and their exosomes improve function, restore mitochondrial integrity and reverse degenerative changes in the hearts of Mdx mice. Circ. Res. *115*, e90.

Aminzadeh, M.A., Durvasula, P., Tobin, R., Guan, X., Andres, A., Taylor, D., Ibrahim, A., Sun, B., Torrente, A., and Goldhaber, J. (2015a). Exosome-mediated reversal of Duchenne cardiomyopathy. Circulation *132*, A16015.

Aminzadeh, M.A., Tseliou, E., Sun, B., Cheng, K., Malliaras, K., Makkar, R.R., and Marbán, E. (2015b). Therapeutic efficacy of cardiosphere-derived cells in a transgenic mouse model of non-ischaemic dilated cardiomyopathy. Eur. Heart J. *36*, 751–762.

Ascheim, D., and Jefferies, J.L. (2016). A randomized, open-label study of the safety and efficacy of multi-vessel intracoronary delivery of allogeneic cardiosphere-derived cells in patients with cardiomyopathy secondary to Duchenne muscular dystrophy. https://clinicaltrials.gov/ct2/show/NCT02485938.

Bao, J.L., and Lin, L. (2014). MiR-155 and Mir-148a reduce cardiac injury by inhibiting NF-kappaB pathway during acute viral myocarditis. Eur. Rev. Med. Pharmacol. Sci. *18*, 2349–2356.

Bentzinger, C.F., Wang, Y.X., and Rudnicki, M.A. (2012). Building muscle: molecular regulation of myogenesis. Cold Spring Harb. Perspect. Biol. *4*, a008342.

Burelle, Y., Khairallah, M., Ascah, A., Allen, B.G., Deschepper, C.F., Petrof, B.J., and Des Rosiers, C. (2010). Alterations in mitochondrial function as a harbinger of cardiomyopathy: lessons from the dystrophic heart. J. Mol. Cell. Cardiol. *48*, 310–321.

Carlson, C.G., Samadi, A., and Siegel, A. (2005). Chronic treatment with agents that stabilize cytosolic IκB-α enhances survival and improves resting membrane potential in MDX muscle fibers subjected to chronic passive stretch. Neurobiol. Dis. *20*, 719–730.

Cheng, K., Malliaras, K., Li, T.-S., Sun, B., Houde, C., Galang, G., Smith, J., Matsushita, N., and Marbán, E. (2012). Magnetic enhancement of cell retention, engraftment, and functional benefit after intracoronary delivery of cardiac-derived stem cells in a rat model of ischemia/reperfusion. Cell Transplant. *21*, 1121–1135.

Chimenti, I., Smith, R.R., Li, T.S., Gerstenblith, G., Messina, E., Giacomello, A., and Marbán, E. (2010). Relative roles of direct regeneration versus paracrine effects of human cardiosphere-derived cells transplanted into infarcted mice. Circ. Res. *106*, 971–980.

Clusin, W.T. (2008). Mechanisms of calcium transient and action potential alternans in cardiac cells and tissues. Am. J. Physiol. Heart Circ. Physiol. *294*, H1–H10.

Davis, D.R., Zhang, Y., Smith, R.R., Cheng, K., Terrovitis, J., Malliaras, K., Li, T.S., White, A., Makkar, R., and Marbán, E. (2009). Validation of the cardiosphere method to culture cardiac progenitor cells from myocardial tissue. PLoS One *4*, e7195.

Gallet, R., Dawkins, J., Valle, J., Simsolo, E., de Couto, G., Middleton, R., Tseliou, E., Luthringer, D., Kreke, M., Smith, R.R., et al. (2017). Exosomes secreted by cardiosphere-derived cells reduce scarring, attenuate adverse remodelling, and improve function in acute and chronic porcine myocardial infarction. Eur. Heart J. *38*, 201–211.

Guan, X., Mack, D.L., Moreno, C.M., Strande, J.L., Mathieu, J., Shi, Y., Markert, C.D., Wang, Z., Liu, G., and Lawlor, M.W. (2014). Dystrophin-deficient cardiomyocytes derived from human urine: new biologic reagents for drug discovery. Stem Cell Res. *12*, 467–480.

Ibrahim, A.G.-E., Cheng, K., and Marbán, E. (2014). Exosomes as critical agents of cardiac regeneration triggered by cell therapy. Stem Cell Reports *2*, 606–619.

Jefferies, J., Byrne, B., Taylor, M., Lima, J., Smith, R.R., Maliaris, K., Fedor, B., Rudy, J., Pogoda, J., Marban, L., et al. (2017). Cardiosphere-derived cells for the treatment of Duchenne cardiomyopathy: results of the Halt cardiOmyopathy ProgrEssion [HOPE]-Duchenne Trial. Circulation *136*, e448.

Kegel, M. (2017). Capricor set to launch phase 2 trial of cell therapy CAP-1002 in advanced DMD patients. Muscular Dystrophy News Today. https://musculardystrophynews.com/2017/12/01/fda-clears-capricor-phase-2-trial-dmd-therapy-cap-1002/.

Lässer, C., Eldh, M., and Lötvall, J. (2012). Isolation and characterization of RNA-containing exosomes. J. Vis. Exp., e3037.

Lee, S.-T., White, A.J., Matsushita, S., Malliaras, K., Steenbergen, C., Zhang, Y., Li, T.S., Terrovitis, J., Yee, K., and Simsir, S. (2011). Intramyocardial injection of autologous cardiospheres or cardiosphere-derived cells preserves function and minimizes adverse ventricular remodeling in pigs with heart failure post-myocardial infarction. J. Am. Coll. Cardiol. *57*, 455–465.

Lee, Y., Andaloussi, S.E., and Wood, M.J. (2012). Exosomes and microvesicles: extracellular vesicles for genetic information transfer and gene therapy. Hum. Mol. Genet. *21*, R125–R134.

Li, T.S., Cheng, K., Malliaras, K., Smith, R.R., Zhang, Y., Sun, B., Matsushita, N., Blusztajn, A., Terrovitis, J., and Kusuoka, H. (2012). Direct comparison of different stem cell types and subpopulations reveals superior paracrine potency and myocardial repair efficacy with cardiosphere-derived cells. J. Am. Coll. Cardiol. *59*, 942–953.

Li, T.S., Cheng, K., Lee, S.T., Matsushita, S., Davis, D., Malliaras, K., Zhang, Y., Matsushita, N., Smith, R.R., and Marbán, E. (2010). Cardiospheres recapitulate a niche-like microenvironment rich in stemness and cell-matrix interactions, rationalizing their enhanced functional potency for myocardial repair. Stem Cells *28*, 2088–2098.

Lötvall, J., Hill, A.F., Hochberg, F., Buzás, E.I., Di Vizio, D., Gardiner, C., Gho, Y.S., Kurochkin, I.V., Mathivanan, S., Quesenberry, P., et al. (2014). Minimal experimental requirements for definition of extracellular vesicles and their functions: a position statement from the International Society for Extracellular Vesicles. J. Extracell. Vesicles *3*, 29613.

Love, D., Morris, G., Ellis, J., Fairbrother, U., Marsden, R., Bloomfield, J., Edwards, Y., Slater, C., Parry, D., and Davies, K. (1991). Tissue distribution of the dystrophin-related gene product and expression in the mdx and dy mouse. Proc. Natl. Acad. Sci. USA *88*, 3243–3247.

Makkar, R., Schatz, R., Traverse, J., Hamer, A., Beattie, K., Smith, R.R., Kivel, F., Marbán, L., Marbán, E., and Henry, T.D. (2014). ALLogeneic heart STem cells to Achieve myocardial Regeneration (ALLSTAR): the one year Phase I results. Circulation *130*, A20536.

Makkar, R.R., Smith, R.R., Cheng, K., Malliaras, K., Thomson, L.E., Berman, D., Czer, L.S., Marbán, L., Mendizabal, A., and Johnston, P.V. (2012). Intracoronary cardiosphere-derived cells for heart regeneration after myocardial infarction (CADUCEUS): a prospective, randomised phase 1 trial. Lancet *379*, 895–904.

Malliaras, K., Li, T.S., Luthringer, D., Terrovitis, J., Cheng, K., Chakravarty, T., Galang, G., Zhang, Y., Schoenhoff, F., and Van Eyk, J. (2012). Safety and efficacy of allogeneic cell therapy in infarcted rats transplanted with mismatched cardiosphere-derived cells. Circulation *125*, 100–112.

Malliaras, K., Makkar, R.R., Smith, R.R., Cheng, K., Wu, E., Bonow, R.O., Marbán, L., Mendizabal, A., Cingolani, E., and Johnston, P.V. (2014). Intracoronary cardiosphere-derived cells after myocardial infarction: evidence of therapeutic regeneration in the final 1-year results of the CADUCEUS trial (CArdiosphere-Derived aUtologous stem CElls to reverse ventricULar dySfunction). J. Am. Coll. Cardiol. *63*, 110–122.

Marbán, E. (2018). The secret life of exosomes: what bees can teach us about next-generation therapeutics. J. Am. Coll. Cardiol. *71*, 193–200.

Martin, D., Rojo, A.I., Salinas, M., Diaz, R., Gallardo, G., Alam, J., de Galarreta, C.M.R., and Cuadrado, A. (2004). Regulation of heme oxygenase-1 expression through the phosphatidylinositol 3-kinase/AKT pathway and the NRF2 transcription factor in response to the antioxidant phytochemical carnosol. J. Biol. Chem. *279*, 8919–8929.

Menazza, S., Blaauw, B., Tiepolo, T., Toniolo, L., Braghetta, P., Spolaore, B., Reggiani, C., Di Lisa, F., Bonaldo, P., and Canton, M. (2010). Oxidative stress by monoamine oxidases is causally involved in myofiber damage in muscular dystrophy. Hum. Mol. Genet. *19*, 4207–4215.

Nagaya, N., Kangawa, K., Itoh, T., Iwase, T., Murakami, S., Miyahara, Y., Fujii, T., Uematsu, M., Ohgushi, H., and Yamagishi, M. (2005). Transplantation of mesenchymal stem cells improves cardiac function in a rat model of dilated cardiomyopathy. Circulation *112*, 1128–1135.

Rogers, R.G., Fournier, M., Aminzadeh, M.A., Gouin, K., Sanchez, L., and Marban, E. (2017). Abstract 16576: intravenous infusion of cardiosphere-derived cells and their exosomes improve dystrophin-deficient cardiomyopathy in mdx mice. Circulation *136*, A16576.

Schiaffino, S., and Mammucari, C. (2011). Regulation of skeletal muscle growth by the IGF1-AKT/PKB pathway: insights from genetic models. Skelet. Muscle *1*, 1.

Shen, D., Cheng, K., and Marbán, E. (2012). Dose-dependent functional benefit of human cardiosphere transplantation in mice with acute myocardial infarction. J. Cell. Mol. Med. *16*, 2112–2116.

Shirokova, N., and Niggli, E. (2013). Cardiac phenotype of Duchenne muscular dystrophy: insights from cellular studies. J. Mol. Cell. Cardiol. *58*, 217–224.

Smith, R.R., Barile, L., Cho, H.C., Leppo, M.K., Hare, J.M., Messina, E., Giacomello, A., Abraham, M.R., and Marbán, E. (2007). Regenerative potential of cardiosphere-derived cells expanded from percutaneous endomyocardial biopsy specimens. Circulation *115*, 896–908.

Tandon, A., Villa, C.R., Hor, K.N., Jefferies, J.L., Gao, Z., Towbin, J.A., Wong, B.L., Mazur, W., Fleck, R.J., and Sticka, J.J. (2015). Myocardial fibrosis burden predicts left ventricular ejection fraction and is associated with age and steroid treatment duration in Duchenne muscular dystrophy. J. Am. Heart Assoc. *4*, e001338.

Tseliou, E., Pollan, S., Malliaras, K., Terrovitis, J., Sun, B., Galang, G., Marbán, L., Luthringer, D., and Marbán, E. (2013). Allogeneic cardiospheres safely boost cardiac function and attenuate adverse remodeling after myocardial infarction in immunologically mismatched rat strains. J. Am. Coll. Cardiol. *61*, 1108–1119.

van Putten, M., Hulsker, M., Young, C., Nadarajah, V.D., Heemskerk, H., van der Weerd, L., t Hoen, P.A., van Ommen, G.J., and Aartsma-Rus, A.M. (2013). Low dystrophin levels increase survival and improve muscle pathology and function in dystrophin/utrophin double-knockout mice. FASEB J. *27*, 2484–2495.

Verhaert, D., Richards, K., Rafael-Fortney, J.A., and Raman, S.V. (2011). Cardiac involvement in patients with muscular dystrophies magnetic resonance imaging phenotype and genotypic considerations. Circ. Cardiovasc. Imaging *4*, 67–76.

Vyas, N., and Dhawan, J. (2016). Exosomes: mobile platforms for targeted and synergistic signaling across cell boundaries. Cell. Mol. Life Sci. *74*, 1567–1576.

Webber, J., and Clayton, A. (2013). How pure are your vesicles? J. Extracell. Vesicles *2*, 19861.

Wehling-Henricks, M., Jordan, M.C., Gotoh, T., Grody, W.W., Roos, K.P., and Tidball, J.G. (2010). Arginine metabolism by macrophages promotes cardiac and muscle fibrosis in mdx muscular dystrophy. PLoS One *5*, e10763.

White, A.J., Smith, R.R., Matsushita, S., Chakravarty, T., Czer, L.S., Burton, K., Schwarz, E.R., Davis, D.R., Wang, Q., and Reinsmoen, N.L. (2013). Intrinsic cardiac origin of human cardiosphere-derived cells. Eur. Heart J. *34*, 68–75.

Williams, I.A., and Allen, D.G. (2007). The role of reactive oxygen species in the hearts of dystrophin-deficient mdx mice. Am. J. Physiol. Heart Circ. Physiol. *293*, H1969–H1977.

Zabeo, D., Cvjetkovic, A., Lasser, C., Schorb, M., Lotvall, J., and Hoog, J.L. (2016). Exosomes purified from a single cell type have diverse morphology and composition. bioRxiv https://doi.org/10.1101/094045.

Stem Cell Reports, Volume *10*

Supplemental Information

Exosome-Mediated Benefits of Cell Therapy in Mouse and Human Models of Duchenne Muscular Dystrophy

Mark A. Aminzadeh, Russell G. Rogers, Mario Fournier, Rachel E. Tobin, Xuan Guan, Martin K. Childers, Allen M. Andres, David J. Taylor, Ahmed Ibrahim, Xiangming Ding, Angelo Torrente, Joshua M. Goldhaber, Michael Lewis, Roberta A. Gottlieb, Ronald A. Victor, and Eduardo Marbán

Figure S1. *Related to Figure 1; Changes in ventricular volumes and engraftment with alterations in transcriptomic and proteomic profiles underlying CDC injection in the mdx heart.*

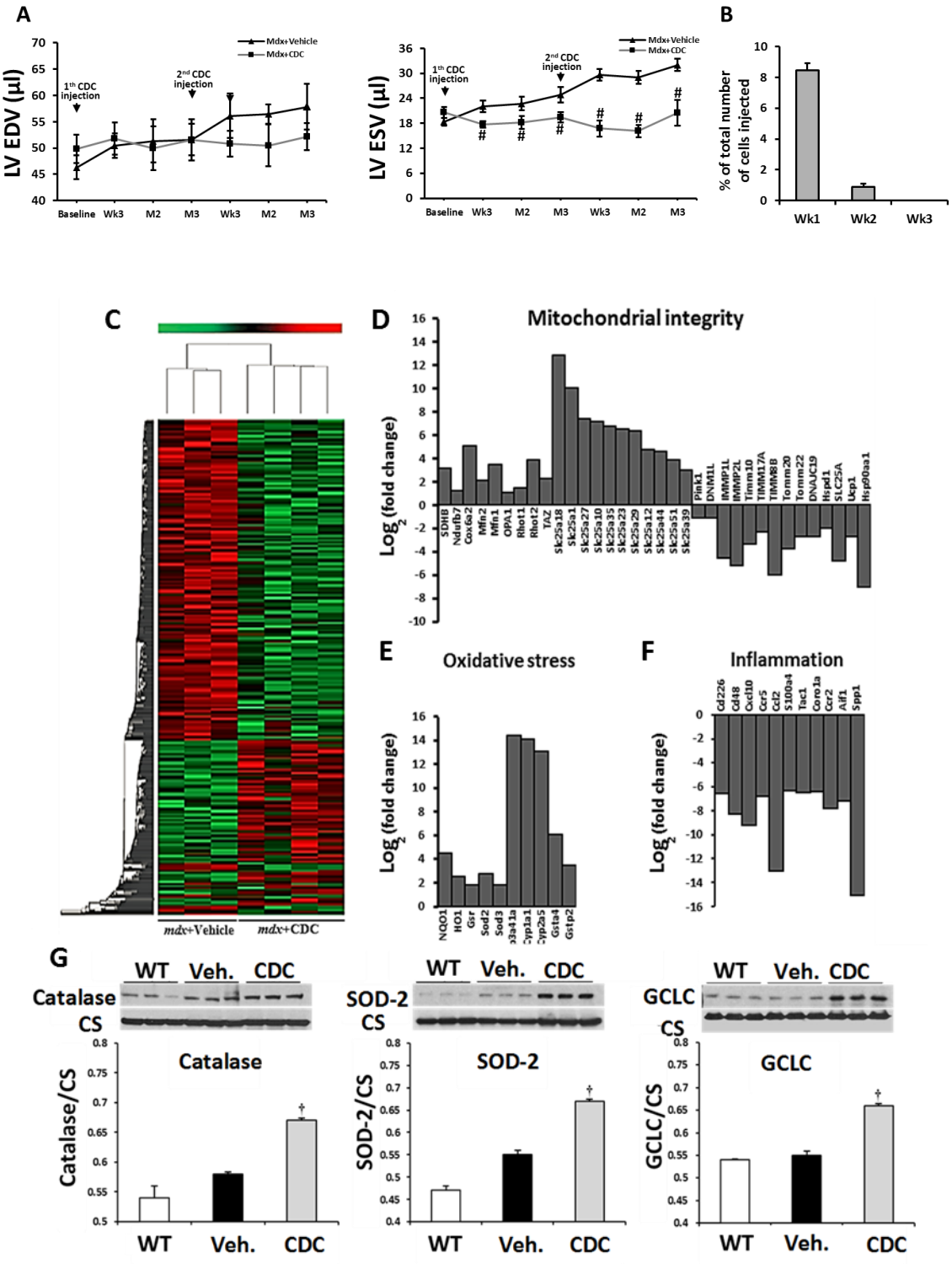

A: Left ventricular end-diastolic (LV EDV) and end-systolic (LV ESV) volumes after cardiosphere-derived cell (CDC) administration. CDC transplantations resulted in a sustained improvement of LV ESV for 3 months after both first and second (3 months interval) injections in *mdx* mice (Mdx+CDC), relative to placebo (Mdx+Vehicle). Differences in LV EDV were more marked after the second injection but were not significant. B: Percentage engraftment of CDCs in the heart 1, 2 and 3 weeks after transplantation. Percentage engraftment of CDCs at 1 week was ~8% and <1% at 2 weeks. By 3 weeks, no surviving CDCs could be detected. n = 3 at each time point. C: Changes in *mdx* heart transcriptome 3 wks after CDC treatment. 2-Dimensional hierarchical clustering using 560 genes with at least 2-fold differences between *mdx* hearts injected with vehicle (Mdx+Vehicle) or CDCs (Mdx+CDC) (A). Each column represents an *mdx* heart and each row a gene. Probe set signal values were normalized to the mean across *mdx* hearts. The relative level of gene expression is depicted from the lowest (green) to the highest (red), according to the scale shown on top. Examples of fold changes of transcripts for genes involved in the various pathways of interest are plotted in panels D-F. G: Western blots and pooled data for protein abundance of catalase, superoxide dismutase-2 (SOD-2), and catalytic subunit of glutamate-cysteine ligase (GCLC) in wild-type (WT) or *mdx* mouse hearts 3 weeks after administration of vehicle (Veh.) or CDCs (CDC). CS: Citrate synthase loading control. *Data are means ± SEM; #P<0.05 vs. Mdx+CDC; †P<0.05 vs. Mdx+Vehicle and WT (wild type).*

Figure S2. *Related to Figure 1; Diminished cardiac fibrosis and collagen content and differential expression of genes involved in inflammation 3 weeks after CDC injection in* mdx *hearts.*

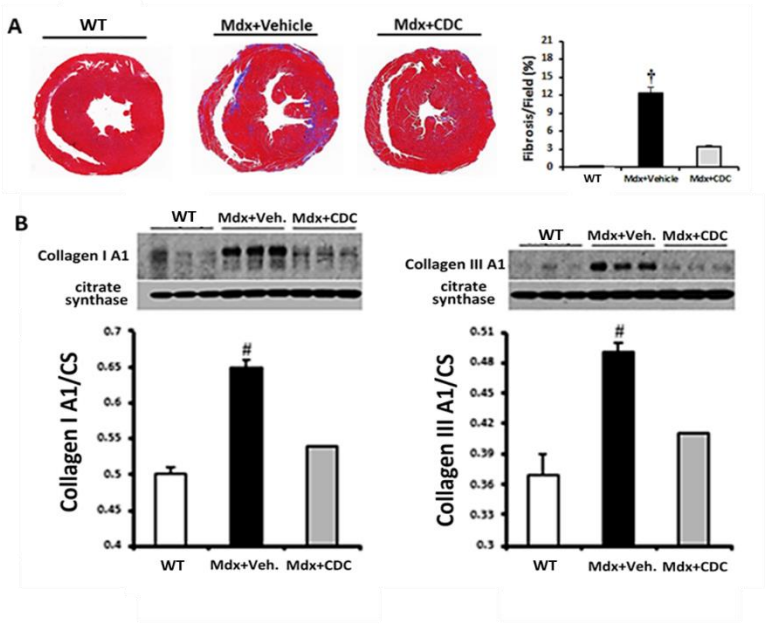

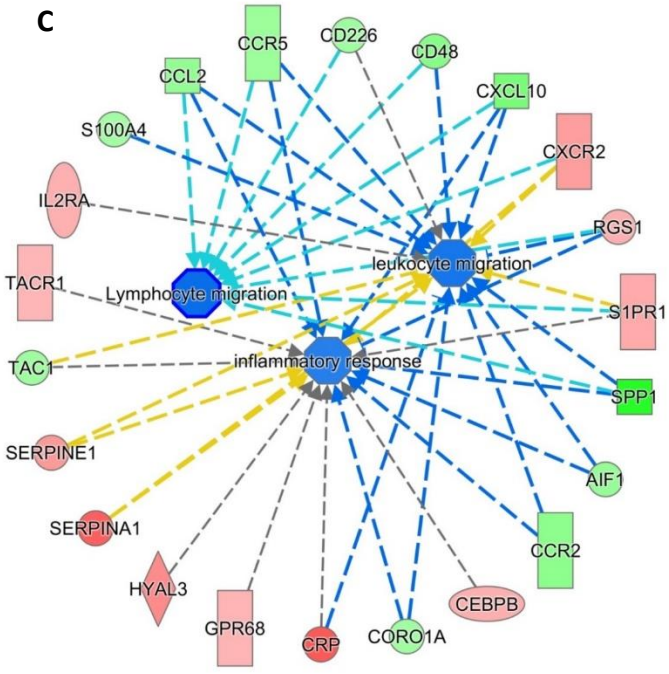

A, left panel: Representative Masson trichrome images of a wild-type heart (WT), an *mdx* heart that had been vehicle-injected (Mdx+Vehicle) and an *mdx* heart that had been CDC-injected (Mdx+CDC). A, right panel: pooled data for morphometric analysis. B: western blots and pooled data for myocardial cardiac collagen IA1 and IIIA1. C: Ingenuity pathway analysis of differentially expressed genes involved in inflammation in CDC/Vehicle *mdx* hearts, denoting inhibition of inflammatory response concomitantly with reduced migration of inflammatory cells in *mdx* hearts 3 weeks after CDC treatment. The blue color represents inhibition of function/response and the red and green colors represent up and downregulation, respectively. Data are means ± SEM; †$P<0.05$ vs. Mdx+CDC and WT (wild type); #$P<0.05$ vs. Mdx+CDC and WT (wild type); Scale Bar: 1mm.

Figure S3. *Related to Figure 1; Numbers of mitochondria from TEM images, mitochondrial DNA copy numbers (per nuclear genome) and cardiomyogenesis in* mdx *heart tissue 3 weeks after injection with vehicle (Veh.) or CDCs.*

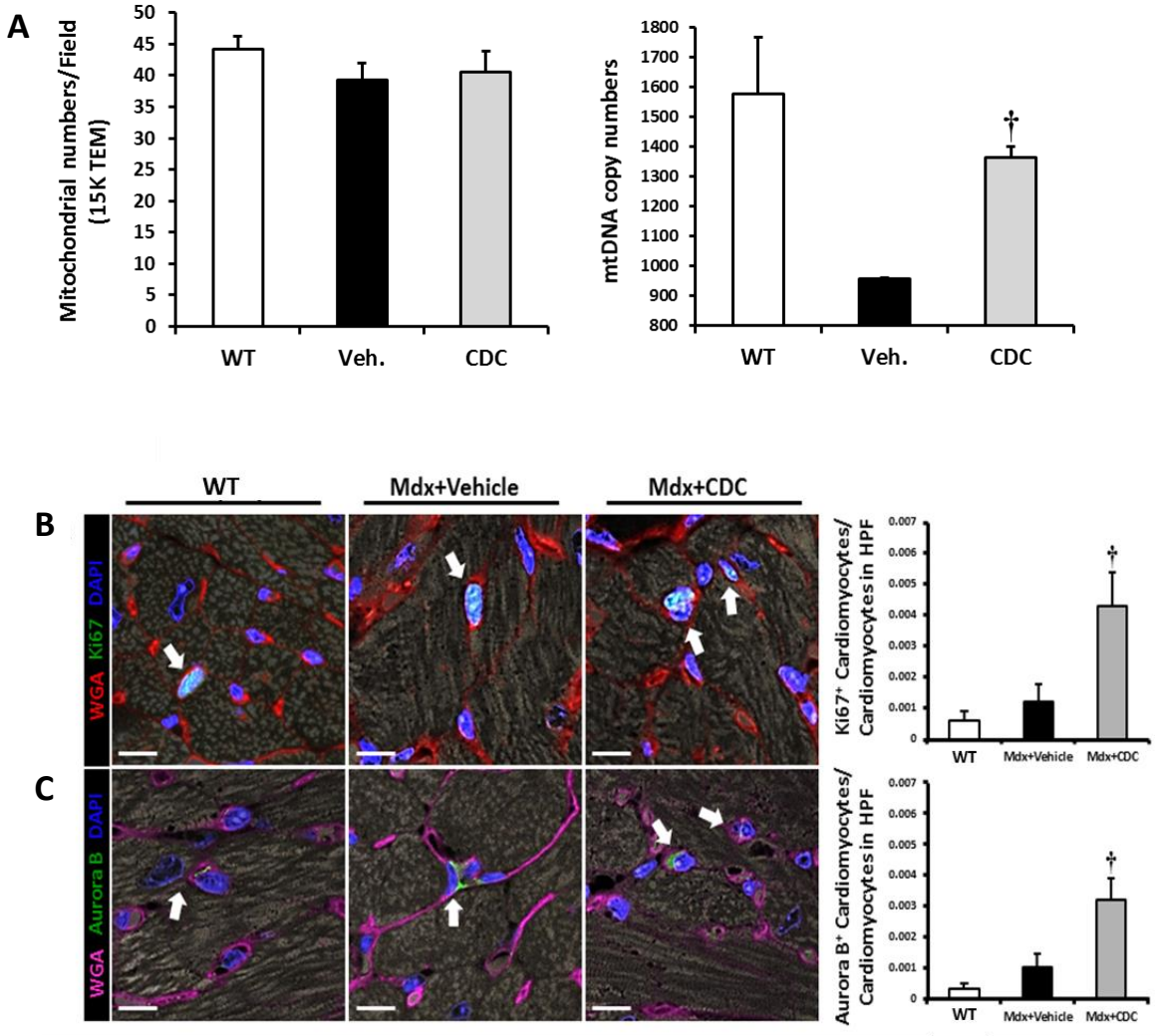

Numbers of mitochondria from TEM images (A; left panel) and mitochondrial DNA copy numbers (per nuclear genome) in *mdx* heart tissue (A; right panel) 3 weeks after injection with vehicle (Veh.) or CDCs. WT: age-matched wild-type mouse hearts. Enhanced cardiomyogenesis 3 weeks after CDC injection in *mdx* mice is evident from representative immunohistochemical images and pooled data (WT [wild type], vehicle- [Mdx+Vehicle] and CDC-treated [Mdx+CDC] *mdx* mouse hearts stained for Ki67 [B] and Aurora B [C]; n=4-6 per group). Arrows point to $Ki67^+$ (B) and aurora B^+ (C) cardiomyocytes. HPF: high power field. Data are means ± SEM; †$P<0.05$ vs. Mdx+Vehicle and WT (wild type); Scale bars: 10µm.

Fig. S4. *Related to Figure 2; Properties of exosomes isolated by ultracentrifugation from hypoxic CDCs: size distributions, physiological responses and immunogenicity.*

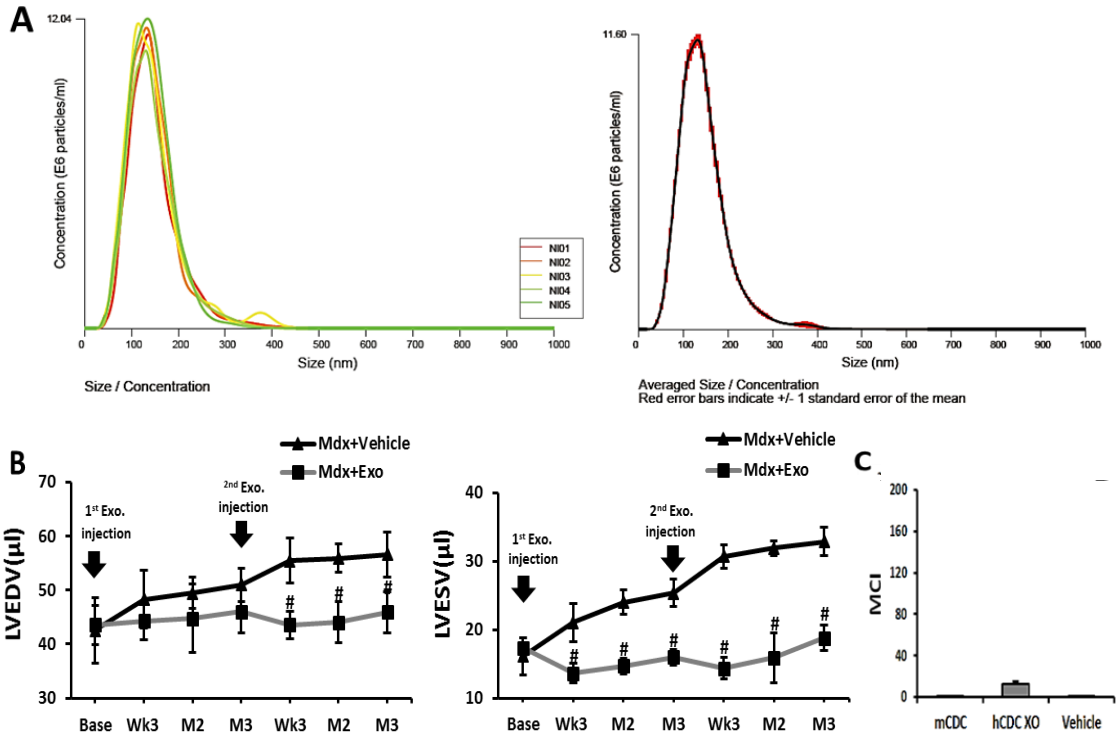

A: Exosomes isolated by ultracentrifugation were analyzed by nanoparticle tracking, using the NanoSight NS300 system (NanoSight Ltd, UK). Videos were collected and analyzed using NTA-software (version 2.3), with the minimal expected particle size, minimum track length, and blur setting all set to automatic. Camera shutter speed was fixed at 30.01 ms and camera gain was set to 500. Camera sensitivity and detection threshold were set close to maximum (15 or 16) and minimum (3 or 4), respectively, to reveal small particles. Ambient temperature was recorded manually, ranging from 24 to 27°C. For each sample, five videos of 60 seconds duration were recorded, with a 10-second delay between recordings, generating five replicate histograms that were averaged. Representative five replicate histograms depicting size/concentration (A; left graph). Standard error of the mean concentration, calculated from 5 replicates, is shown in red in right graph. B: LV end-diastolic (LV EDV) and end-systolic (LV ESV) volumes after CDC exosome (Exo) administration. CDC-exosome transplantation resulted in a sustained improvement of LV ESV for 3 months after both first and second (3 months later) injections in *mdx* muse hearts relative to placebo. Differences in LV EDV were significant only after the second injection. C: IgG serum levels 6 months after the first injection and 3 months after repeat injection of mouse CDCs (mCDC), human CDC exosomes (hCDC XO) and vehicle in *mdx* mice. Circulating anti-donor IgG antibodies were screened by flow cytometry. Pooled data are means ± SEM. # *P<0.001* vs Mdx+Exo.

Figure. S5. *Related to Figure 3; Secondary effects of intramyocardial CDC injection on remote tissues.*

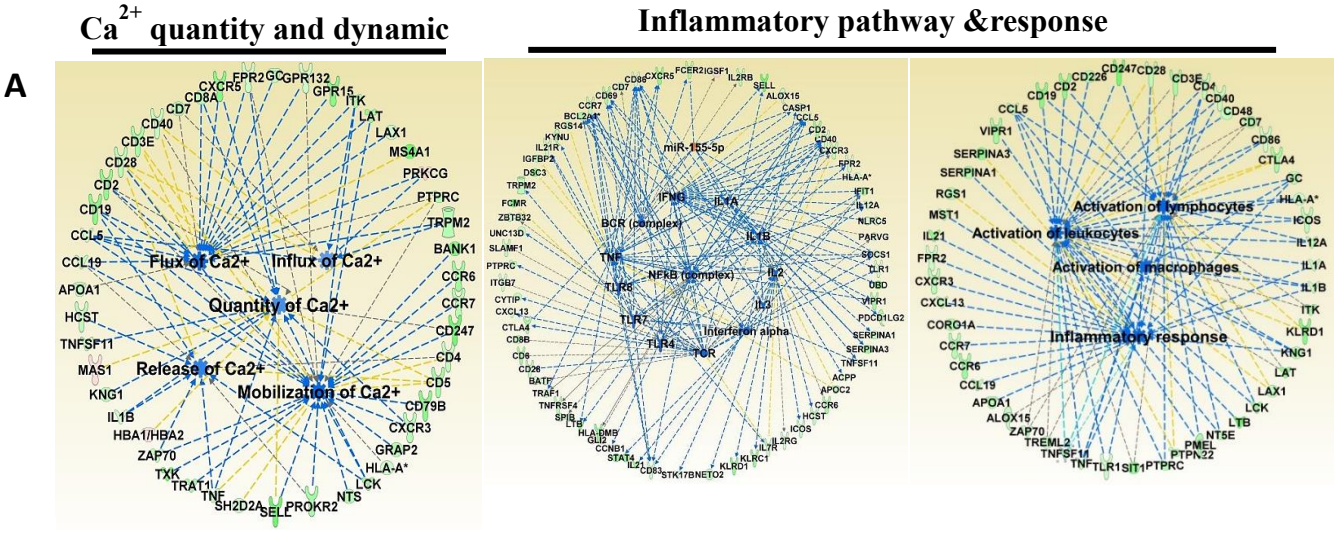

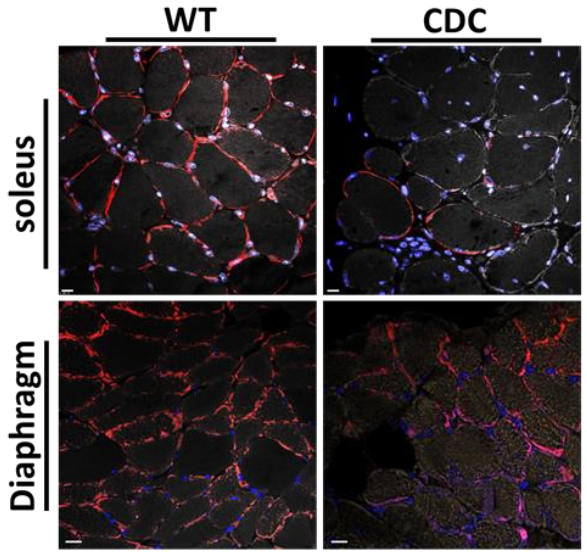

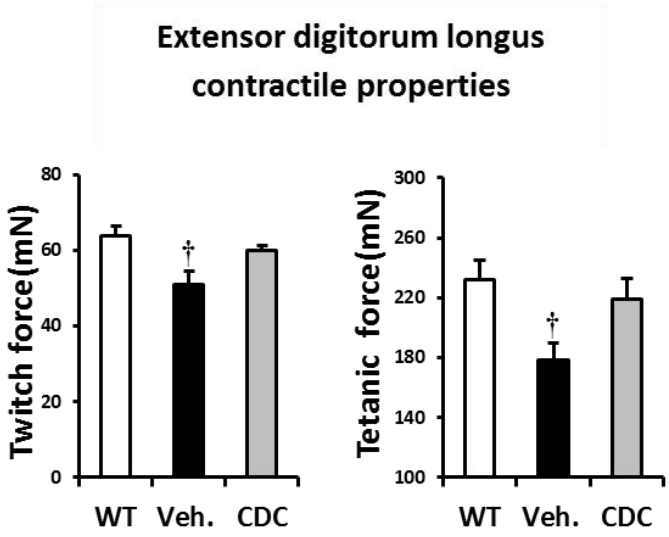

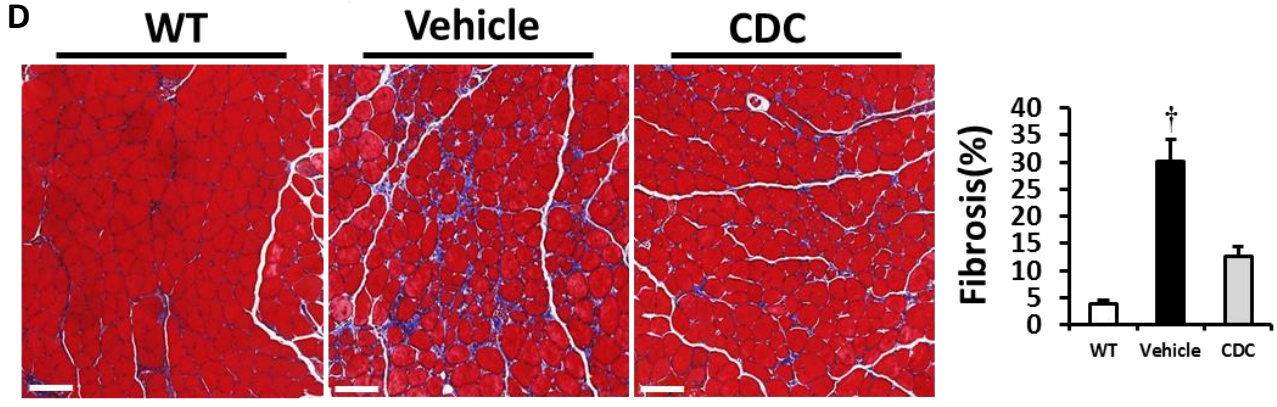

A: Ingenuity pathway analysis of differentially expressed genes involved in Ca^{2+} dynamics and inflammation in diaphragm of *mdx* mice treated intramyocardially with CDC or vehicle, denoting improved Ca^{2+} dynamic and inhibition of NF-κB inflammatory pathway and inflammation in *mdx* diaphragm. Blue color represents inhibition of function/response and the red and green colors represent up and downregulation, respectively. B: Dystrophin expression in soleus and diaphragm muscles of *mdx* mice 3 weeks after treatment. Representative immunohistochemical images of soleus and diaphragm from wild type control (WT) and *mdx* mice intramyocardially-injected with CDCs (CDC) stained for dystrophin. C: Extensor digitorum longus (EDL) contractile properties after intramyocardial CDC injection: *In vitro* measurement of EDL isometric twitch force and maximum tetanic force in controls (WT) and 3 weeks after injection of vehicle (Veh.) or CDCs (CDC) into *mdx* hearts. D: Diminished fibrosis in *mdx* soleus muscles 3 weeks after intramyocardial CDC injection (CDC) relative to vehicle; WT: wild-type control. Representative Masson trichrome images (left) and pooled data for morphometric analysis. *Data are means ± SEM; †P<0.005 vs. CDC and WT (control); Scale bars: 10μm (B); 100 μm (D).*

Figure S6. *Related to Figure 3 and Figure 4; Non-cardiac manifestations of CDC or CDC exosome injections and fold changes of microRNAs in CDC exosomes isolated from hypoxic conditioned media compared to CDC exosomes isolated from normoxic conditioned media.*

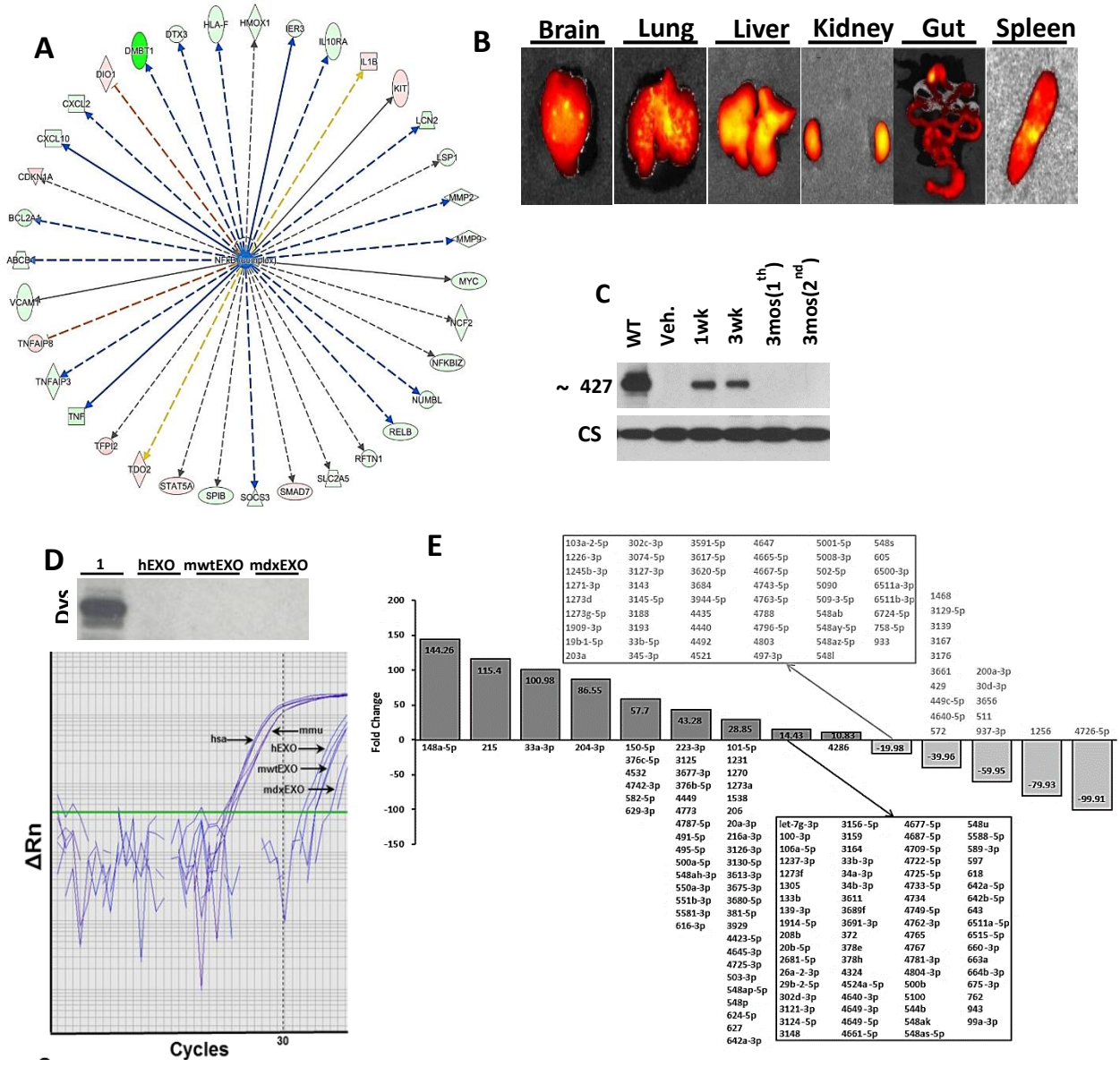

A: Ingenuity pathway analysis of differentially expressed genes involved in inflammation in liver of *mdx* mice injected intramyocardially with CDCs or vehicle, showing inhibition of NF-κB inflammatory pathway in *mdx* livers 3 weeks after intramyocardial CDC injection. The blue color represents inhibition of function/response and the red and green colors represent up and downregulation, respectively. B: Bioluminescence imaging of *mdx* mouse organs after systemic injection of dyed human CDC exosomes. Six hours after injection of exosomes systemically into the *mdx* mouse left ventricular cavity, the indicated organs were dissected and imaged using IVIS molecular imaging systems (Caliper Life Sciences, Hopkinton, MA, USA). C: Western blot of dystrophin protein in wild type control (WT) mouse heart and *mdx* mouse hearts 1 week, 3 weeks and 3 months after first intraventricular CDC-exosome injection and 3 months after second (repeat) CDC-exosome injection. D: Immunoblot probing for full length dystrophin protein in CDC-exosomes from human (hEXO), wild-type mouse (mwtEXO), and *mdx* mouse (mdxEXO). No detection of dystrophin protein in exosomes isolated from any CDC source. E: qPCR reaction for dystrophin on human (hsa) and mouse (mmu) heart tissues (positive controls) and on exosomes isolated from human CDCs (hEXO), mouse wild-type CDCs (mwtEXO), and *mdx* mouse CDCs (mdxEXO). All reactions for CDC-exosomes were flagged for empty well, demonstrated dystrophin mRNA below detection limits by quantitative PCR. F: Fold changes of microRNAs in CDC exosomes isolated from hypoxic conditioned media (2% O_2) compared to CDC exosomes isolated from normoxic conditioned media; fold change >10 and <-20 were included. NEBNext Small RNA Library Prep kit (New England BioLabs, Ipswich, MA) was used for miRNA-seq library preparation of extracted small RNAs from the exosomes. RNAs were extracted from exosomes using miRNeasy Serum/Plasma Kit (QIAGEN, Germantown, MD).

Figure S7. *Related to Figure 7; Sashimi plots of RNA-Seq data for dystrophin from WT (wild type) and vehicle-, CDC-, CDC-exosome- and miR-148a treated* mdx *hearts and verification that the bioactivity of the extracellular vesicles studied here is indeed attributable to exosomes characterized by the most rigorous of criteria.*

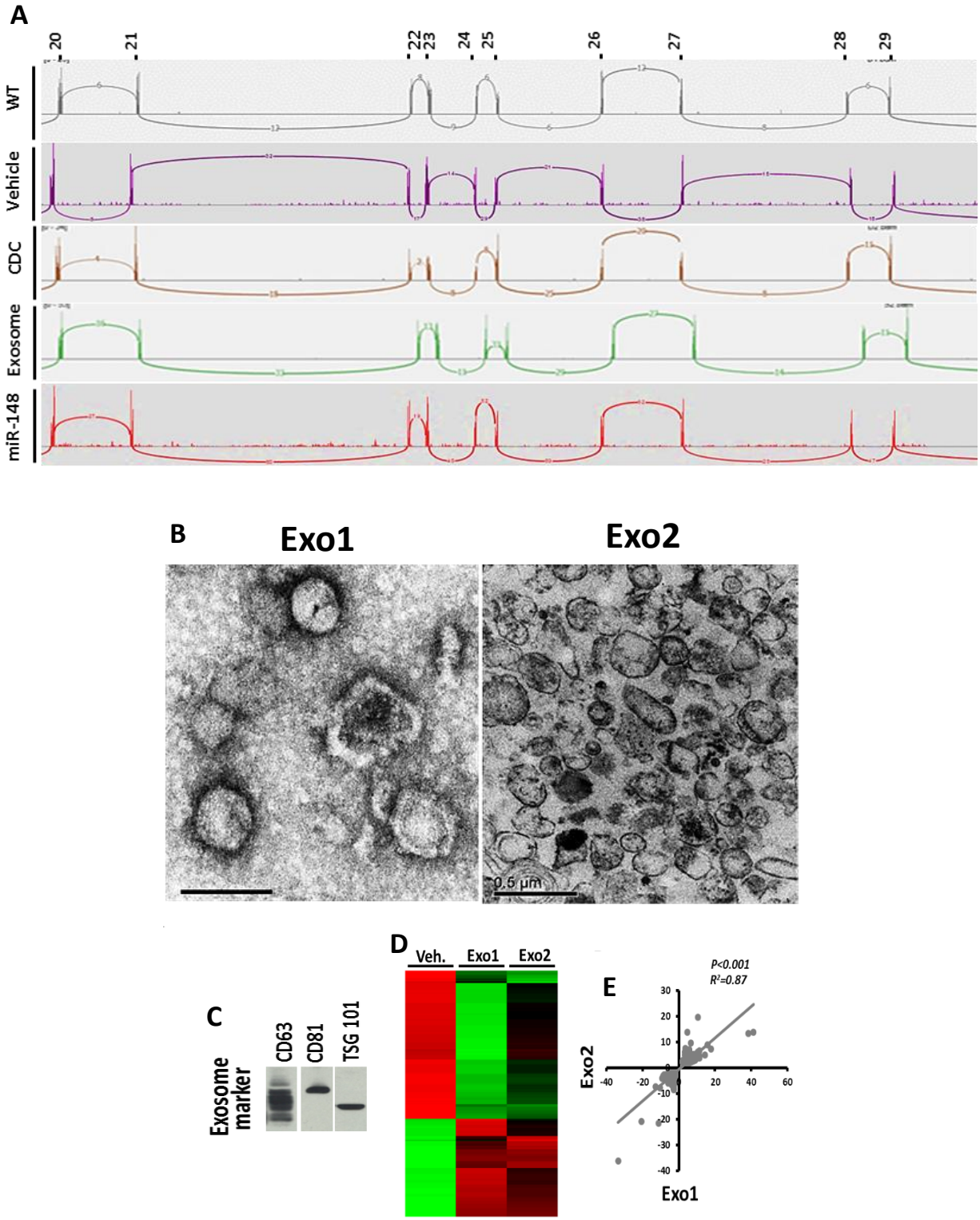

A: Sashimi plots of RNA-Seq data for dystrophin from WT (wild type) and vehicle-, CDC-, CDC-exosome- and miR-148a treated *mdx* hearts depict no junction read spanning exon 23. B-E: Verification that the bioactivity of the extracellular vesicles studied here are indeed attributable to exosomes characterized by the most rigorous of criteria (Lötvall et al., 2014). We floated the exosomes on a linear iodixanol density gradient, demonstrated vesicles by transmission electron microscopy (TEM) and the presence of key membrane proteins, and show that the biological effect truly is vesicle associated. B: TEM images of sequentially-centrifuged exosomes with (Exo1, left) and without (Exo2, right) purification with linear iodixanol density gradient show vesicles in both conditions. The vesicles are variable in size and morphology, consistent with previous work (Zabeo et al., 2016). C: Western blot on lysed exosomes for key proteins characteristic of exosomes: CD63, CD81 and TSG. D: Biological activity of Exo1 and Exo2 were compared by injection into *mdx* soleus muscles and evaluation of *mdx* soleus transcriptome 3 weeks after injection. Changes in *mdx* soleus transcriptome 3 wks after Exo1 and Exo2 injection. 2-Dimensional hierarchical clustering using 332 genes with at least 2-fold differences between vehicle/Exo1 and vehicle/Exo2 in *mdx* soleus muscles. E: Correlation of fold changes in expression of same genes 3 weeks after Exo1 and Exo2 injection in *mdx* soleus muscles. The similarity of the effects of Exo1 and Exo2 support the notion that the bioactivity of the vesicles isolated by our default protocol (cf. Fig. S9) is genuinely due to exosomes, and not to other types of vesicles that might have been co-purified by ultracentrifugation; Scale bars: 50μm (Exo1); 100 nm (Exo2).

Assessment of CDC engraftment and dystrophin mRNA in exosomes by real-time polymerase chain reaction

Quantitative polymerase chain reaction (PCR) was performed 1, 2 and 3 weeks after CDC injection to assess cell engraftment. Male CDCs were injected into female *mdx* mice to enable detection of the SRY gene located on the Y chromosome as a marker of engraftment using the TaqMan assay (Applied Biosystems, Foster City, CA)(Li et al., 2012). The whole mouse heart was harvested, weighed, and homogenized. A standard curve was generated with multiple dilutions of genomic DNA isolated from the same batch of CDCs injected. All samples were spiked with equal amounts of genomic DNA from non-injected mouse hearts as a control. For each reaction, 50 ng of genomic DNA was used. Real-time PCR was performed in triplicate. Engraftment was quantified from the standard curve. Percentage engraftment of CDCs at 1 week was ~8% and <1% at 2 weeks. By 3 weeks, no surviving CDCs could be detected. **Dystrophine mRNA in exosomes:** Standard Sybr green qPCR reactions were setup starting with 500 ng of cDNA from human (hsa) and mouse (mmu) heart tissues (positive controls) and from exosomes isolated from human CDCs (hEXOs), mouse wild-type CDCs (mwtEXO), and *mdx* mouse CDCs (mdxEXOs). Average Ct values were figas follows: hsa control (23.4), mmu control (24.0), hEXO (33.8), mwtEXO (35.0), mdxEXO (36.8). All reactions for CDC-exosomes were flagged for empty well. Primers for all qPCR reactions are listed in panel below.

Gene	Accession No.	Sequence (5' → 3')
DMD (mmu)	XM_006527767	F: TCAGTCCAGAAGCCCATGAAC R: GGACAAAACCCACTCGCTAGA
DMD (hsa)	NM_004006	F: GTCCCTCTCTGCGTGGATATG R: CCGCTTCGATCTCTGGCTTAT

Respirometry

Mice were sacrificed via cervical dislocation after isofluorane anesthesia. Hearts were immediately excised, rinsed in PBS and homogenized via polytron in 1mL ice cold HES buffer (250mM sucrose, 1mM EDTA, 10mM HEPES, pH 7.4). Lysates were spun down at 1000*g* for 5min at 4^{o}C to remove unbroken cells and large debris. Supernatant was then spun down at 7000*g* for 10min at 4^{o}C to separate mitochondria-enriched fraction from crude cytosol. The pellet was resuspended in 1mL HES buffer (A subportion in lysis buffer for WB). Protein quantification was performed and adjusted with HES buffer to obtain sample containing 10µg protein in 50µL buffer which was loaded into a 24-well Seahorse cell culture plate, which was spun down at 2000*g* for 20min at 4^{o}C to allow mitochondria to adhere to the plate surface. 450µL MAS buffer (70mM sucrose, 220mM mannitol, 5mM KH2PO4, 5mM MgCl2, 1mM EGTA, 0.2% fatty acid-free BSA, pH 7.4) was then added prior to Seahorse XF24 mitochondria stress test. 5mM/5mM pyruvate/malate and 0.25mM ADP were used to stimulate mitochondrial oxidative phosphorylation followed by 1µM oligomycin, 1µM FCCP, and a mixture of 1µM antimycin, 500nM rotenone. Citrate synthase activity was measured in sample lysates to normalize for the actual amount of mitochondria loaded for the test. Seahorse respirometry on normal and Duchenne iPS cell-derived cardiomyocytes was performed using Seahorse™ XF96 Extracellular Flux analyzer as described (Guan et al., 2014).

Bioluminescence imaging of *mdx* mouse organs after systemic injection of fluorescently-labeled CDC-exosomes

Six hours after injection of fluorescently-labeled CDC-exosomes systemically into the *mdx* mouse left ventricular cavity, the mice were sacrificed and the organs dissected and imaged using an IVIS molecular imaging system (Caliper Life Sciences, Hopkinton, MA, USA).

Intracellular Ca^{2+} recordings

iPS- derived cardiomyocytes were loaded for 30 min with 5 μM of the fluorogenic calcium-sensitive dye, Cal-520 (AAT Bioquest, Sunnyvale, CA) and paced via field stimulation at a frequency of 1 Hz using an Ion-Optix Myopacer (IonOptix Corp) delivering 0.2 ms square voltage pulses with an amplitude of 20 V via two platinum wires placed on each side of the chamber base (~1 cm separation). We used the xyt mode (2D) of a Leica TCS-SP5-II (Leica Microsystems Inc.; Wetzlar, Germany) to image intracellular Ca^{2+}. Cal- 520 was excited with a 488 nm laser and its emission (>505 nm) was collected with a 10X objective (Leica: N PLAN 10x/0.25) at scan speeds ranging from 36 to 7 ms per frame depending on the field size. The fluorescence intensity (F) proportional to Ca^{2+} concentration was normalized to baseline fluorescence, F0 (F/F0). Time to peak and Ca^{2+} transient amplitude (F/F0) were analyzed with the software Clampfit (ver. 10.2, Molecular Devices, Inc.). Beat-to-beat alternans in each group was calculated over 5-10 sec intervals of pacing at 1 Hz. The amplitude of each transient from each cell (n=10 cells in each group) was measured during pacing and mean and standard deviation were compared among groups.

RNA sequencing and 2-Dimensional hierarchical clustering

Nugen Ovation RNA-Seq System V2 kit was used to generate double-stranded cDNA using a mixture of random and poly (T) priming. Kapa LTP library kit (Kapa Biosystems, Wilmington MA) was used to make the sequencing library. The workflow consists of fragmentation of double stranded cDNA, end repair to generate blunt ends, A-tailing, adaptor ligation and PCR amplification. Different adaptors were used for multiplexing samples in one lane. Sequencing was performed on Illumina HiSeq 2500 for a pair read 100 run. Data quality check was done on

Illumina SAV. Demultiplexing was performed with Illumina CASAVA 1.8.2. The reads were first mapped to the latest UCSC transcript set using Bowtie2 version 2.1.0 and the gene expression level was estimated using RSEM v1.2.15 (Accession number: GSE85888). TMM (trimmed mean of M-values) was used to normalize the gene expression. Differentially expressed genes were identified using the edgeR program. Genes showing altered expression with $p<0.05$ and more than 2 fold changes were considered differentially expressed. The pathway and network analyses were performed using Ingenuity pathway analysis (IPA). IPA computes a score for each network according to the fit of the set of supplied focus genes. These scores indicate the likelihood of focus genes to belong to a network versus those obtained by chance. A score > 2 indicates ~99% confidence that a focus gene network was not generated by chance alone. The canonical pathways generated by IPA are the most significant for the uploaded data set. Fischer's exact test with FDR option was used to calculate the significance of the canonical pathway. 2-Dimensional hierarchical clustering used genes with at least 2 times fold change difference (log_2) between vehicle/CDC, mutant/CDC-exosome (intraventricular injection) or CDC (intramyocardial)/ CDC-exosome (intraventricular injection) *mdx* hearts, diaphragms, soleus and EDL muscles. Each column represents an *mdx* analyzed tissue and each row a gene. Probe set signal values were normalized to the mean across *mdx* analyzed tissues. The relative level of gene expression is depicted from the lowest (green) to the highest (red), according to the scale shown; examples of fold changes of transcripts for genes involved in the various pathways of interest are plotted.

Cardiac mitochondria after intramyocardial CDC injection

TEM images of sections from apical, middle and basal parts of each heart were used for calculating the average numbers of mitochondria in WT (wild type) and CDC/vehicle *mdx* mouse hearts. Extracted DNAs (QIAamp DNA Mini Kit, QIAGEN, Germantown, MD) from whole heart tissue

were used to measure mitochondrial to nuclear DNA ratio using PCR format per manufacturer's instructions (NovaQUANT™ Mouse Mitochondrial to Nuclear Ratio kit, EMD Millipore, Billerica, MA).

Authentication

The CDC cell lines were authenticated by karyotype, antigenic, phenotype, and PCR viral and mycoplasma assessments. The pluripotency of the iPSCs was confirmed by 1) PCR array of pluripotency associated genes; 2) immunostaining for critical pluripotent markers such as OCT-4, SOX-2, SSEA4 and Tra-1-60, Tra-1-81. 3) teratoma assay by engrafting iPS in the kidney capsule of SCID mice.

Echocardiography

Echocardiographic studies were performed two days before (Baseline) and 3 weeks, 2 and 3 months after first CDC/CDC-exosome (CDC-exosome) or vehicle injection and 3 weeks, 2 and 3 months after second CDC/CDC-exosome or vehicle injection (when applicable) using the Vevo 770 Imaging System (VisualSonics, Toronto, Canada)(Smith et al., 2007). The same imaging system was used to perform echocardiographic studies at baseline (2 days before) and 3 weeks after selected RNA (or control) injection. After induction of light general anesthesia, the heart was imaged at the level of the greatest LV diameter. LV ejection fraction (LVEF) was measured with VisualSonics version 1.3.8 software from 2-dimensional long-axis views.

Treadmill exercise testing and survival analysis

For Fig. 1B, exercise capacity was assessed weekly with Exer-3/6 open treadmill (Columbus Instruments, Columbus, OH), beginning 1 week pre-operatively and 3 weeks after CDC/vehicle

injection (exercise capacity measured in a subset of *mdx* mice 1 week pre-operatively was equivalent to that measured 3 weeks post-operatively in the Mdx+Vehicle group). After an acclimation period (10 m/min for 20 min), stepwise increases in average speed (2 m/min) were applied every two minutes during treadmill exercise until the mouse became exhausted (spending >10 seconds on shocker; continuous nudging was used during treadmill to help mice stay on the track). Subsequently, the mouse was returned to the cage and the total distance recorded. The treadmill protocol conformed to guidelines from the American Physiological Society(Kregel et al., 2006). After 3 months of weekly exercise, CDC/vehicle *mdx* mice along with wild-type age-matched mice were followed for assessment of mortality (Fig. 1C).

In vitro isometric contractile properties of skeletal muscle

Mice were deeply anesthetized with Ketamine/Xylazine (80 mg/kg and 10 mg/kg body weight IP), the soleus (SOL) and/or extensor digitorum longus (EDL) and/or diaphragm (DIA) muscles were rapidly excised, and the animal was euthanized. Briefly, following a lateral midline skin incision of the lower leg the SOL and/or EDL muscle was dissected and isolated and its tendons of origin and insertion were tightened with silk suture (3-0) and rapidly excised. The SOL or EDL muscle was vertically mounted in a tissue bath containing a mammalian Ringer's solution of the following composition: (in mM) 137 NaCl, 5 KCl, 2 $CaCl_2$, 1 $MgSO_4$, 1 NaH_2PO_4, 24 $NaHCO_3$, 11 glucose. The solution was constantly aerated with 95% O_2 and 5% CO_2 with pH maintained at 7.35 and temperature kept at 24°C. For studies of the diaphragm, following a left costal margin skin and muscle incision, a section of the midcostal hemidiaphragm was transferred to a preparatory Sylgar-lined dish containing cold Ringer’s and a narrow 3-4 mm wide strip of diaphragm was isolated maintaining fiber attachments to the rib and central tendon intact which were tighten with silk suture and mounted vertically in the tissue bath. One end of the SOL, EDL or DIA was secured to

a clamp at the bottom of the dish and one end was attached to a calibrated force transducer (Cambridge Technology Model 300B, Watertown, MA). A micromanipulator linked to the system was used to adjust muscle length. Platinum plate electrodes placed on each side of the muscle were used for direct muscle stimulation (Grass Model S88 stimulator; Quincy, MA) using 0.2 msec duration monophasic rectangular pulses of constant current delivered at supramaximal intensity. Muscle length was adjusted until maximum isometric twitch force responses were obtained. Isometric contractile properties were determined at optimal length (Lo). Peak twitch force (Pt) was determined from a series of single pulses. Force/frequency relationships were measured at stimulus frequencies ranging from 5-150 pulses per second (pps). The stimuli were presented in trains of 1 sec duration with an interval of at least 1 min intervening between each stimulus train. Muscle forces generated, including Pt and maximum tetanic force (Po), were normalized for the estimated physiological cross-sectional areas (CSA) of the muscle segment (CSA = muscle weight/1.056 x Lo; where 1.056 g/cm^3 represents the density of muscle) and expressed in Newtons (N)/cm^2. For the SOL and EDL muscle Lo was also normalized for muscle fiber length (0.71 and 0.44 of Lo, respectively) in estimating muscle specific force. Absolute muscle forces generated by the SOL and EDL are also reported (mN)(Fournier and Lewis, 2000).

Histology

Mice were sacrificed 3 weeks (WT: n=4; Mdx+Vehicle: n=6; Mdx+CDC/Mdx+CDC-exosome: n=6 each) or 3 months (WT: n=4; Mdx+Vehicle: n=6; Mdx+CDC/Mdx+CDC-exosome: n=6) after first CDC/CDC-exosome injections (n=6). Paraffin-embedded sections from apical, middle and basal parts of each heart or from diaphragm or entire soleus muscle (cross or longitudinal sections) were used for histology. Masson's trichrome staining (HT15 Trichrome Stain [Masson] Kit; Sigma-Aldrich, St. Louis, MO) was performed for evaluation of fibrosis. T cells, B cells and

macrophages were assessed by immunostaining with antibodies against mouse CD3, CD20 and CD68, respectively, and the average number of cells was calculated by counting cells in 10 fields from each of 10 sections selected randomly from the apical (3 sections; 50µm interval), middle (4 sections; 50µm interval) and basal (3 sections; 50µm interval) regions of each heart or from diaphragm. The data were presented as number of cells/mm^2 field. Actively-cycling ($Ki67^+$) and proliferating (Aurora B^+) cardiomyocytes were counted in the same manner, and the cycling and proliferating fractions were expressed as the number of $Ki67^+$, Aurora B^+ divided by the total number of cardiomyocytes per high-power field (HPF), respectively, as described(Aminzadeh et al., 2015). Measurements were averaged for each heart. Immunofluorescence staining: Heat-induced epitope retrieval in low or high pH buffer (DAKO, Carpinteria, CA) was followed by 2 hours permeabilization/blocking with Protein Block Solution (DAKO, Carpinteria, CA) containing 1% saponin (Sigma, St. Louis, MO; Protein Block Solution contained 3% saponin was applied for immunofluorescence staining of Ki67). Subsequently, primary antibodies in Protein Block Solution were applied overnight in 4 C° for immunofluorescence staining of 5-µm sections from apical, middle and basal parts of each heart or cross sections of soleus muscle. After 3x wash with PBS, each 10 minutes, Alexa Fluor secondary antibodies (Life Technologies, Grand Island, NY) were used for detection. Images were taken by a Leica TCS SP5 X confocal microscopy system. Immunofluorescence staining was conducted using antibodies against Ki-67 (SP6; RM-9106-S0; 1:50, Thermo Fisher Scientific, Fremont, CA), WGA (Wheat germ agglutinin; W32466, 1:200; Thermo Fisher Scientific, Fremont, CA), Nrf2 (C20; 1:50; Santa Cruz Biotechnology, Santa Cruz, CA), aurora B (611082; 1:250; BD Biosciences, San Jose, CA). Immunoperoxidase staining: Immunohistochemical detection of CD3 (AC-0004A), CD20 (AC-0012A) and CD68 (790-2931) was performed on 5-µm sections using prediluted rabbit monoclonal antibodies from Ventana

Medical System (Tuscon, AZ; CD68) and Cell Marque (Rocklin, CA; CD3, CD20). Staining was conducted on the Leica Bond-Max Ventana automated slide stainer (Chicago, IL) using onboard heat-induced epitope retrieval method in high pH ER2 buffer (Leica Biosystems, Buffalo Grove, IL). Staining was visualized using the Dako Envision^{+} rabbit detection System and Dako DAB (Carpinteria, CA). The slides were subsequently counterstained with mayer's hematoxylin for 1 minute and coverslipped. Electron microscopy: Apical (1 cube), middle (3 cubes from right, middle and left subparts) and basal (3 cubes from right, middle and left subparts) parts of posterior wall from each heart (WT: n=3; Mdx+Vehicle: n=3; Mdx+CDC: n=3) were fixed by immersion of 1mm^3 cubes in 2% glutaraldehyde, postfixed in osmium, and embedded in epon. Sections were cut at silver thickness, stained with uranyl acetate and lead citrate, and viewed with JEOL 1010 equipped with AMT digital camera system.

Western blots

Western blot analysis was performed to compare abundance of target proteins contributing to Nrf2 signaling [Nrf2, phospho-Nrf2 (Nrf2-p^{s40}) and Nrf2 downstream gene products: heme oxygenase-1 (HO-1), catalase, superoxide dismutase-2 (SOD-2), and catalytic subunit of glutamate-cysteine ligase (GCLC)], Nrf2 phosphorylation [phospho-Akt(Akt-p^{308}; Akt-p^{473})], oxidative phosphorylation [CI (NDUFB8 subunit), CII (SDHB subunit), CIV (MTCO1 subunit), CIII (UQCRC2 subunit) and CV (ATPSA subunit)], inflammation (NF-κB and MCP-1), fibrosis (Collagen IA1 and collagen IIIA1) and myofiber proliferation and differentiation (Myogenin, MyoD and IGF1R). Density of malondialdehyde protein adducts, a marker of oxidative stress, was also measured by Western blotting (WB). Samples from apical, middle and basal parts of each heart (each 1 mm-thick transverse section) were mixed and homogenized, and nuclear and cytoplasmic fractions were extracted per manufacturer's instructions (CelLytic NuCLEAR

Extraction Kit, Sigma-Aldrich, St. Louis, MO). The same kit was applied for extraction of nuclear and cytoplasmic fractions from entire soleus muscle, a narrow 3-4 mm wide strip of the left midcostal hemidiaphragm and iPSC derived cardiomyocytes. Mitochondria were extracted from fresh whole hearts (WT: n=3; Mdx+Vehicle: n=8; Mdx+CDC: n=8) as described in respirometry section. Cytoplasmic, nuclear and mitochondrial extracts for WB analysis were stored at −80C°. The protein concentrations in extracts were determined by the Micro BCA Protein Assay Kit (Life technologies, Grand Island, NY). Target proteins in the cytoplasmic, nuclear and mitochondrial fractions were measured by Western blot analysis using the following antibodies: antibodies against mouse Nrf2 (C-20; sc-722) , HO-1 (H-105; sc-10789), catalase (H-300; sc-50508), SOD-2 (FL-222; sc-30080), GCLC (H-338; sc-22755), collagen IA1 (D-13; sc-25974), and collagen IIIA1 (S-17; sc-8780-R) were purchased from Santa Cruz Biotechnology (Santa Cruz, CA), phospho-Nrf2 (Nrf2-p^{s40}; orb34864; Biorbyt, San Francisco, CA), respiratory chain subunits (Total OXPHOS Rodent WB Antibody Cocktail antibody; MS604), malondialdehyde (ab27642), citrate synthase (ab96600) and TBP (TATA binding protein; ab63766) [Abcam, Cambridge, MA], Akt (9272) and Akt-p^{T308} (5106S) , IκB-α (4814S), p-IκB-α (9246S), phospho-NF-κB p65 (Ser536; 3033S) [Cell Signaling Technology, Denver, CO], MCP-1 (HPA019163), NF-κB p65 (SAB4502615) [Sigma-Aldrich, St. Louis, MO], Myogenin (F12B; MA5-11658), MyoD (5.8A; MA1-41017), Akt-p^{S47} (14-6; OMA1-03061) and IGF-IR/IGF1 Receptor (194Q13; AHO1292) [Thermo Fischer Scientific, Fremont, CA] antibodies were purchased from the cited sources. Antibodies to TBP and citrate synthase were used for measurements of the housekeeping proteins for nuclear (TBP), cytosolic and mitochondrial (citrate synthase) target proteins. Western blot methods: Briefly, aliquots containing 20 μg proteins were fractionated on 8, 10 and 4-12% Bis-Tris gel (Life technologies, Grand Island, NY) at 120 V for 2 h and transferred to a PVDF

membrane (Life technologies, Grand Island, NY). The membrane was incubated for 1 h in blocking buffer (1× TBS, 0.05% Tween-20 and 5% nonfat milk) and then overnight in the same buffer containing the given antibodies at optimal dilutions. The membrane was washed 3 times for 5 min in 1× TBS, 0.05% Tween-20 before a 2-h incubation in a buffer (1× TBS, 0.05% Tween-20 and 3% nonfat milk) containing horseradish peroxidase-linked anti-rabbit IgG (7074P2), anti-mouse IgG (7076S) [Cell Signaling Technology, Denver, CO] and anti-goat IgG (A5420; Sigma-Aldrich, St. Louis, MO) at 1:1000-3000 dilution. The membrane was washed 3 times for 5 min in 1 × TBS, 0.05% Tween-20 and developed by autoluminography using the ECL chemiluminescent agents (Super Signal West Pico Chemiluminescent Substrate; Life Technologies, Grand Island, NY). Citrate synthase and TBP were used as housekeeping proteins against which expressions of the proteins of interest were normalized. Phosphorylated Akt, Nrf2 and IκB-α were normalized to total Akt, Nrf2 and IκB-α. Western blot analyses of collagen I and collagen III were conducted under non-reducing, non-denaturing conditions.

Statistical analysis

All pooled data are presented as mean±SEM, except results for alternans data (Fig. 6A) which are presented as mean ±SD. Normality and equality of variances of data sets were first tested using Kolmogorov-Smirnov and Levene's tests, respectively. If both were confirmed, t-test or analysis of variance followed by Bonferroni's post hoc test were used for determination of statistical significance; if either normality or equality of variances was not assured, nonparametric tests (Wilcoxon test or Kruskal-Wallis test followed by Dunn's post-test) were applied (SPSS II, SPSS Inc., Chicago, Illinois). No preliminary data were available for a power analysis. Results from a pilot project allowed us to power subsequent studies. The study followed preclinical reporting standards, as described (Landis et al., 2012). Age-matched mice were randomly allocated to

experimental groups using computer generated randomization schedules (https://www.randomizer.org). Conduct of experiments and analysis of results and outcomes were performed in a blinded manner (allocation concealment and blinded assessment of outcome). There was no post-hoc exclusion of mice or data after the analysis before unblinding.

Ejection Fraction Data

Preliminary data were collected from a pilot study of 5 animals per group measuring ejection fraction at baseline, and again 3 weeks after treatment with cells or vehicle control in *mdx* and corresponding wild-type mice (C57BL/10ScSnJ). The measured treatment effect was approximately 4 units, with a time effect of approximately 1 unit, with group standard deviations of 3.5 units. We anticipated larger differences between groups over later time points with possible increase in measured variance. Therefore, with 12 animals per treatment group in the each of the *mdx* groups, and 7 wild-type control animals, the study had at least 80% power to detect a difference of 4.5 units or greater in treatment effect and 1.4 units or greater in time effect in a study design with 6 measurements per animal over time assuming a compound symmetry covariance structure, a correlation of 0.7 between measurements within animals over time, and a two-sided alpha of 0.05. (Power computed via PASS v. 11.0.).

Treadmill Data

Preliminary data were collected from a pilot study of 5 animals per group measuring treadmill distance (i.e., the distance ambulated before exhaustion, as described below) at baseline, and again 3 weeks after treatment with cells or vehicle control in *mdx* animals and corresponding wild-type animals. The measured treatment effect was approximately 150 meters, with limited differences observed over time in untreated groups. Group standard deviations were approximately 75 meters,

with more variation observed after treatment. We anticipated larger differences between groups over later time points with possible increase in measured variance. Therefore, with 11 animals per treatment group in the each of the transgenic groups, and 7 wild-type control animals, the study had at least 80% power to detect a difference of 100 meters or greater in treatment effect and changes of at least 30 meters over time in a study design with 12 measurements per animal over time assuming a compound symmetry covariance structure, a correlation of 0.7 between measurements within animals over time, and a two-sided alpha of 0.05. (Power computed via PASS v. 11.0.).

REFERENCES

Aminzadeh, M.A., Tseliou, E., Sun, B., Cheng, K., Malliaras, K., Makkar, R.R., and Marbán, E. (2015). Therapeutic efficacy of cardiosphere-derived cells in a transgenic mouse model of non-ischaemic dilated cardiomyopathy. European heart journal *36*, 751-762.

Fournier, M., and Lewis, M.I. (2000). Functional, cellular, and biochemical adaptations to elastase-induced emphysema in hamster medial scalene. Journal of Applied Physiology *88*, 1327-1337.

Guan, X., Mack, D.L., Moreno, C.M., Strande, J.L., Mathieu, J., Shi, Y., Markert, C.D., Wang, Z., Liu, G., and Lawlor, M.W. (2014). Dystrophin-deficient cardiomyocytes derived from human urine: new biologic reagents for drug discovery. Stem cell research *12*, 467-480.

Kregel, K.C., Allen, D.L., Booth, F.W., Fleshner, M.R., Henriksen, E.J., Musch, T., O'Leary, D., Parks, C., Poole, D., and Ra'anan, A. (2006). Resource book for the design of animal exercise protocols. American Physiological Society Bethesda, 1-80.

Landis, S.C., Amara, S.G., Asadullah, K., Austin, C.P., Blumenstein, R., Bradley, E.W., Crystal, R.G., Darnell, R.B., Ferrante, R.J., and Fillit, H. (2012). A call for transparent reporting to optimize the predictive value of preclinical research. Nature *490*, 187-191.

Li, T.-S., Cheng, K., Malliaras, K., Smith, R.R., Zhang, Y., Sun, B., Matsushita, N., Blusztajn, A., Terrovitis, J., and Kusuoka, H. (2012). Direct comparison of different stem cell types and subpopulations reveals superior paracrine potency and myocardial repair efficacy with cardiosphere-derived cells. Journal of the American College of Cardiology *59*, 942-953.

Lötvall, J., Hill, A.F., Hochberg, F., Buzás, E.I., Di Vizio, D., Gardiner, C., Gho, Y.S., Kurochkin, I.V., Mathivanan, S., Quesenberry, P.*, et al.* (2014). Minimal experimental requirements for definition of extracellular vesicles and their functions: a position statement from the International Society for Extracellular Vesicles. 2014.

Smith, R.R., Barile, L., Cho, H.C., Leppo, M.K., Hare, J.M., Messina, E., Giacomello, A., Abraham, M.R., and Marbán, E. (2007). Regenerative potential of cardiosphere-derived cells expanded from percutaneous endomyocardial biopsy specimens. Circulation *115*, 896-908.

Zabeo, D., Cvjetkovic, A., Lasser, C., Schorb, M., Lotvall, J., and Hoog, J.L. (2016). Exosomes purified from a single cell type have diverse morphology and composition. bioRxiv.